ATLAS NOTE

ATLAS-CONF-2012-161

November 13, 2012

Search for the Standard Model Higgs boson produced in association with a vector boson and decaying to bottom quarks with the ATLAS detector

The ATLAS Collaboration

Abstract

This note presents an updated search with the ATLAS experiment for the Standard Model Higgs boson produced in association with a W or Z boson and decaying to $b\bar{b}$ using 4.7 fb^{-1} of LHC proton-proton data at $\sqrt{s}$ = 7 TeV and 13.0 fb^{-1} at $\sqrt{s}$ = 8 TeV. The search is performed using events containing zero, one or two electrons or muons targeting the three decay modes $ZH \to \nu\bar{\nu}b\bar{b}$, $WH \to \ell\nu b\bar{b}$ and $ZH \to \ell^+\ell^- b\bar{b}$. No significant excess is observed. For m_H = 125 GeV, the observed (expected) upper 95% confidence level limit on the cross section times the branching ratio is found to be 1.8 (1.9) times the Standard Model prediction. A Standard Model Higgs boson with m_H = 110 GeV is excluded. As a validation of the analysis procedure, the production of diboson pairs, WZ and ZZ, with a Z boson decaying to $b\bar{b}$, has been observed with a significance of 4.0 standard deviations and a rate compatible with the Standard Model expectation.

ATLAS-CONF-2012-161
14 November 2012

1 Introduction

The search for the Standard Model (SM) [1–3] Higgs boson [4–7] is a central component of the physics program at the Large Hadron Collider (LHC). Recently, the observation of a boson decaying to a pair of photons or massive vector bosons has been reported by the ATLAS [8] and CMS [9] collaborations. Determining the nature of this boson - whether it is indeed the Standard Model Higgs boson - is now one of the most important questions in particle physics.

An SM Higgs boson with a mass of about 125 GeV would be accessible in both bosonic and fermionic decay channels at the LHC. Observing the decay into fermions is vital in testing whether the new boson is compatible with a SM Higgs boson. In particular, the decay to b-quarks plays an important role since this is expected to be the dominant decay mode at this mass ($BR(H \to b\bar{b}) \approx 58\%$ [10]). Therefore an observation in this channel is crucial in order to provide a direct constraint on the largest decay mode.

Experiments at the Tevatron have reported an excess of events in the search for the Higgs boson in the $b\bar{b}$ decay mode corresponding to about three standard deviations [11]. The CMS collaboration set expected and observed upper limits on the production cross section times branching ratio of 1.6 and 2.1 times the Standard Model expectation, respectively [9].

This note presents an update of the results reported in Ref. [12] on the search for the Higgs boson decaying to a pair of b-quarks with the Higgs boson produced in association with a W or Z boson, jointly denoted as V, in the decay channels $ZH \to \nu\bar{\nu}b\bar{b}$, $WH \to \ell\nu b\bar{b}$ and $ZH \to \ell^+\ell^- b\bar{b}$, where ℓ refers to either an electron or a muon. The cross section for associated production with W or Z bosons is lower than that of the dominant gluon fusion process by more than an order of magnitude; however, the signature provided by the leptonic decay modes of the associated vector boson is used to reduce backgrounds. The update reported in this note uses 4.7 fb^{-1} of data at $\sqrt{s} = 7$ TeV delivered by the LHC in 2011 and 13.0 fb^{-1} of data at $\sqrt{s} = 8$ TeV delivered by the LHC in 2012. The analysis is performed for events containing zero, one or two leptons, targeting the three Higgs boson decay channels mentioned above. The 0-lepton channel is most sensitive to ZH production, with a small although not insignificant contribution from WH production. The sensitivity of the 1-lepton channel is dominated by WH production with a small contribution from ZH, whereas the 2-lepton channel is only sensitive to ZH production. The channels are split in further categories, depending on the vector boson transverse momentum and the number of jets.

The analysis has been optimised with respect to Ref. [12] to improve the sensitivity. The most important improvements are a re-optimisation of the topological selection criteria for all three channels, increased lepton identification efficiency, the addition of further categories with different signal to background ratios, and improvements to the di-b-jet invariant mass resolution.

2 The ATLAS Detector

The ATLAS detector consists of four main subsystems. An inner tracking detector is immersed in the 2 T magnetic field produced by a superconducting solenoid. Charged particle position and momentum measurements are made by silicon detectors in the pseudorapidity[1] range $|\eta| < 2.5$ and also by a straw tube tracker in the range $|\eta| < 2.0$. Calorimeters cover $|\eta| < 4.9$ with a variety of detector technologies. The liquid-argon electromagnetic calorimeter is divided into barrel ($|\eta| < 1.475$) and endcap ($1.375 < |\eta| < 3.2$) sections. The hadronic calorimeters (using liquid argon or scintillating tiles as active materials)

[1] ATLAS uses a right-handed coordinate system with its origin at the nominal interaction point (IP) in the centre of the detector and the z-axis coinciding with the axis of the beam pipe. The x-axis points from the IP to the centre of the LHC ring, and the y-axis points upward. Cylindrical coordinates (r,ϕ) are used in the transverse plane, ϕ being the azimuthal angle around the beam pipe. The pseudorapidity is defined in terms of the polar angle θ as $\eta = -\ln\tan(\theta/2)$. For the purpose of the fiducial selection, this is calculated relative to the geometric centre of the detector; otherwise, it is relative to the reconstructed primary vertex of each event.

surround the electromagnetic calorimeter and cover $|\eta| < 4.9$. The muon spectrometer measures the deflection of muon tracks in the field of three large air-core toroidal magnets, each containing eight superconducting coils. It is instrumented with separate trigger chambers (covering $|\eta| < 2.4$) and high-precision tracking chambers (covering $|\eta| < 2.7$).

3 Data and Simulation Samples

This analysis uses the full 2011 dataset which consists of 4.7 fb^{-1} [13,14] of LHC data at $\sqrt{s} = 7$ TeV and 13.0 fb^{-1} of 2012 LHC data at $\sqrt{s} = 8$ TeV recorded by the ATLAS detector until September 2012. The data were collected using either lepton or missing transverse energy triggers with quality requirements on the beam conditions and detector performance. The integrated luminosity differs slightly between the different channels due to the availability of the triggers.

Monte Carlo (MC) event samples produced with the full ATLAS detector simulation [15] based on the GEANT4 [16] program, corrected for all known detector effects, are used to model the Higgs boson signal and most backgrounds. The high statistics samples used to model the vector boson plus jet backgrounds were produced using a simulation that includes a full simulation of the inner tracking and muon detectors but uses a fast simulation of the calorimeters based on detailed parametrisations of shower shapes of single particles [17]. The preliminary analysis described here uses a mixture of MC samples from different generators because a consistent set is not yet available.

In the analysis of the $\sqrt{s} = 8$ TeV data the WH and ZH signal processes are modelled using Pythia 8 [18], interfaced using CTEQ6L1 [19] parton distribution functions (PDFs) with the AU2 tune [20] for the parton shower, hadronisation and multiple parton interactions. In the analysis of the $\sqrt{s} = 7$ TeV data the Pythia 6 [21] event generator, interfaced with the MRST modified leading-order (LO*) [22] PDFs, with the AUET2B tune. The total production cross sections and associated uncertainties, computed at next-to-leading order (NLO), are taken from Ref. [23] with additional NLO corrections as a function of the transverse momentum of the vector boson, p_{T}^{V} [24, 25]. The decay branching ratios are calculated with Hdecay [10].

The t-channel single-top process is simulated with AcerMC, interfaced with Pythia 6, while the s-channel and Wt-channel of single-top quark production and the top-quark pair production are simulated with MC@NLO, relying on CT10 NLO PDFs [26], using Herwig [27] for hadronisation.

The Herwig generator is used to simulate the diboson (ZZ, WZ and WW) samples relying on the CTEQ6L1 PDF.

The Powheg [28–30] generator, in combination with MSTW 2008 NLO PDFs [31] for 2011 data and with CT10 NLO PDFs for 2012 data and interfaced with the Pythia 6 program for the parton shower and hadronisation, is used to simulate $W + b$ events. For $W+c$ and $W+$ light jet production the Alpgen generator [32] interfaced with the Herwig program [27] is used.

For 2012 data the $Z + b$, $Z + c$ and $Z+$light jet events are produced with the Sherpa generator [33], interfaced with CTEQ6L1 PDFs, while at $\sqrt{s} = 7$ TeV a combination of Alpgen and Sherpa, with the same settings, is used: $Z + b$, $Z + c$ are produced with Sherpa, while $Z+$light jet is produced with Alpgen.

Simulated jets are categorised according to which hadrons lie within a cone of 0.4 around the jet axis. Simulated $V+$jet events are categorised according to the true flavour of the two reconstructed jets that are used to reconstruct the Higgs boson mass:

- $V + \geq 1$ b events, if at least one of the two jets is a real b-jet
- $V + \geq 1$ c events, if there is no real b-jet, but at least one of the two jets is a real c-jet
- $V + \geq 1$ light events, if neither of the jets is a real b or c-jet.

4 Object and Event Selection

Events are sub-divided into three channels depending on whether they contain zero, one or two leptons. Events in the 0-lepton channel are selected using triggers based on missing transverse energy. Three similar but different trigger configurations were used in the 2012 dataset as the increasing event pile-up necessitated changes to the trigger. Pile-up is the overlapping of events from different proton-proton collisions occurring in the same bunch crossing. Events in the 1- and 2-lepton channels are primarily selected using single lepton triggers. Events selected for the 2-lepton analysis could also be recorded by di-muon or di-electron triggers.

Three categories of leptons are used in the analysis denoted in increasing order of purity as loose, medium and tight leptons. Loose leptons are selected with transverse energy $E_{\mathrm{T}} > 10$ GeV and pass impact parameter and quality requirements. If they are electrons they are required to have $|\eta| < 2.47$. Three types of muons are included in the loose definition to maximise the acceptance: muons reconstructed in both the muon spectrometer and the inner detector cover $|\eta| < 2.5$, muons identified in the calorimeter and associated with an inner detector track are accepted for $|\eta| < 0.1$, where there is limited muon chamber coverage, and muons without a full inner detector track are accepted for $2.5 < |\eta| < 2.7$. Finally, the sum of the transverse momentum of tracks within an $\eta - \phi$ cone of radius 0.2 centred on the lepton candidate track, but excluding the lepton track, is required to be less than 10% of the transverse momentum of the lepton.

Medium leptons meet the loose identification criteria and have $E_T > 25$ GeV. Medium electrons are required to pass additional quality requirements based on the track quality and the shower shape. Tight leptons require the sum of the calorimetric energy deposits in a cone of radius of 0.3 around the lepton, excluding energy associated with the lepton candidate, to be less than 14% of the lepton energy. Tight electrons are required to pass more stringent quality requirements.

Jets are reconstructed from topological 3D clusters in the calorimeters using the anti$-k_{\mathrm{t}}$ algorithm [34] with a radius parameter $R = 0.4$ and are required to have $p_{\mathrm{T}} > 20$ GeV and $|\eta| < 4.5$. Jet energies are calibrated using p_{T} and η-dependent correction factors based on simulation and validated with data [35]. To remove jets from pile-up vertices, the sum of the p_{T} of the tracks from the primary vertex and matched to the jet must be at least 75% (50%) of the total p_{T} summed for all tracks matched to the jet for the $\sqrt{s} = 7$ TeV($\sqrt{s} = 8$ TeV) analysis. The two jets used to reconstruct the Higgs boson candidate are required to satisfy $|\eta| < 2.5$. The leading jet is required to have $p_{\mathrm{T}}^1 > 45$ GeV.

Jets originating from b-quarks are identified using the MV1 b-tagging algorithm [36–39] which combines informations from different algorithms based on the use of track impact parameter significances or explicit reconstruction of b-hadron decay vertices. The two b-tagged jets used to reconstruct the Higgs boson candidate are selected with a cut on the output of this algorithm, which, when evaluated on simulated $t\bar{t}$ events, results in an approximate efficiency of 70% for b-jets and rejection factors of 5 and 150 for c and light jets, respectively.

Simulated jets are categorised according to which hadrons lie within a cone of 0.4 around the jet axis. Jets with a b-hadron in the cone are denoted b-jets, non b-jets with a c hadron are labelled as c-jets, and non-b or c-jets with a τ as τ-jets. All other jets are regarded as light jets.

The statistical uncertainties on the simulated $V + c$ and V+light jet backgrounds are reduced by parametrising the response to b-tagging with the measured c- and light-tagging efficiencies and applying these efficiencies to the full $V+c$ and V+light jet samples to derive the distributions for events containing two tagged jets. A direct cut on the output of the MV1 algorithm is used for simulated events with real b-jets.

The missing transverse energy, $E_{\mathrm{T}}^{\mathrm{miss}}$, is measured as the negative vector sum of the transverse momenta associated with cluster energies in the calorimeters with $|\eta| < 4.9$. Corrections are applied to energy associated with reconstructed objects: jets, electrons, τ-leptons, photons and muons [40]. A

track-based missing transverse momentum, $p_{\mathrm{T}}^{\mathrm{miss}}$, is calculated as the negative vector sum of the transverse momenta of tracks associated to the primary vertex.

The event selection is summarised in Tables 1 and 2. Events containing no loose leptons are assigned to the 0-lepton channel. Events containing one tight lepton and no additional loose leptons are considered to be in the 1-lepton channel. Events containing one medium lepton and one additional loose lepton of the same flavour but of opposite charge are studied in the 2-lepton channel. In the zero lepton channel multijet background is suppressed by imposing cuts on $E_{\mathrm{T}}^{\mathrm{miss}}$, $p_{\mathrm{T}}^{\mathrm{miss}}$, the azimuthal angle between these ($\Delta\phi(E_{\mathrm{T}}^{\mathrm{miss}}, p_{\mathrm{T}}^{\mathrm{miss}})$), the azimuthal angle between the $E_{\mathrm{T}}^{\mathrm{miss}}$ and the nearest jet (Min[$\Delta\phi(E_{\mathrm{T}}^{\mathrm{miss}}$, jet)]) and the azimuthal angle between $E_{\mathrm{T}}^{\mathrm{miss}}$ and the 2 b-tagged jets ($\Delta\phi(E_{\mathrm{T}}^{\mathrm{miss}}, b\bar{b})$). Cuts are made on $E_{\mathrm{T}}^{\mathrm{miss}}$ and m_{T}^{W} in the 1-lepton channel[2] to select events consistent with the presence of a W boson. The top background is reduced in the 2-lepton channel by imposing cuts on the di-lepton invariant mass ($m_{\ell\ell}$) and $E_{\mathrm{T}}^{\mathrm{miss}}$. The transverse momentum of the vector boson, p_{T}^{V}, is reconstructed as the $E_{\mathrm{T}}^{\mathrm{miss}}$ in the 0-lepton channel, the vector sum of the lepton and the $E_{\mathrm{T}}^{\mathrm{miss}}$ in the 1-lepton channel (p_{T}^{W}) and the vector sum of the two leptons in the 2-lepton channel (p_{T}^{Z}).

Events containing zero leptons are split into six categories depending on whether they contain two or three jets and on the missing transverse energy: $120 < E_{\mathrm{T}}^{\mathrm{miss}} \leq 160$ GeV, $160 < E_{\mathrm{T}}^{\mathrm{miss}} \leq 200$ GeV and $E_{\mathrm{T}}^{\mathrm{miss}} > 200$ GeV. Events containing one or two leptons are divided into five categories of p_{T}^{V}: $p_{\mathrm{T}}^{V} \leq 50$ GeV, $50 < p_{\mathrm{T}}^{V} \leq 100$ GeV, $100 < p_{\mathrm{T}}^{V} \leq 150$ GeV, $150 < p_{\mathrm{T}}^{V} \leq 200$ GeV and $p_{\mathrm{T}}^{V} > 200$ GeV.

Topological cuts are applied to enhance the signal and reject backgrounds by exploiting differences in correlations between selected objects. These are outlined in Table 2. These cuts differ between the channels as the different background compositions mandate different selection strategies. The cuts were optimised with respect to Ref. [12] particularly for events with high vector boson transverse momentum. Cuts on the angular separation between the two b-tagged jets, $\Delta R(b, \bar{b}) = \sqrt{\Delta\phi(b, \bar{b})^2 + \Delta\eta(b, \bar{b})^2}$, depend on the category. The minimum cut reduces the background from V+jet production, while the maximum cut is tightened with increasing transverse momentum to profit from the increasing collimation between the jets. In the 1-lepton channel an upper cut on m_{T}^{W} reduces the contamination from the $t\bar{t}$ background. As the multijet background decreases rapidly with increasing p_{T}^{W}, the lower m_{T}^{W} cut is removed from events with $p_{\mathrm{T}}^{W} > 150$ GeV, improving the signal acceptance. Vetoes on jets additional to the two b-tagged jets are applied in the 0-lepton and 1-lepton channels to reject background from $t\bar{t}$ decays.

Events in the signal region are required to contain exactly two b-tagged jets, which are used to reconstruct the mass of the Higgs boson candidate, $m_{b\bar{b}}$. For 3-jet events the leading two jets are required to be b-tagged. The mass resolution is improved by adding the energy from muons within the jet to the total jet energy. A p_{T}-dependent correction is also applied to account for biases in the response caused by resolution effects of the jets from the Higgs boson decay. The average resolution after these corrections is about 16%.

5 Background Normalisation and Control Samples

The dominant backgrounds are top, W+jet and Z+jet production with Z+jet production the largest for the 2-lepton channel, top and W+jets for the 1-lepton channel and all three making an approximately equal contribution to the 0-lepton channel.

Backgrounds are estimated using a combination of techniques based on the comparison of data and MC predictions. The shapes of most background distributions are taken from simulation with the normalisation estimated using control regions in data. The two exceptions are the multijet background, which is estimated using data, and the diboson background for which both the normalisation and shape

[2]The transverse mass (m_{T}) is defined from the transverse momenta and the azimuthal angles of the charged lepton (p_{T}^{ℓ} and ϕ^{ℓ}) and missing transverse momentum, ($E_{\mathrm{T}}^{\mathrm{miss}}$ and ϕ^{miss}): $m_{\mathrm{T}} = \sqrt{2p_{\mathrm{T}}^{\ell}E_{\mathrm{T}}^{\mathrm{miss}}(1 - \cos(\phi^{\ell} - \phi^{\mathrm{miss}}))}$.

Table 1: The basic event selection of the three channels. The details of the cuts on the individual objects are summarised in the text.

Object	0-lepton	1-lepton	2-lepton
Leptons	0 loose leptons	1 tight lepton + 0 loose leptons	1 medium lepton + 1 loose lepton
Jets	2 b-tags $p_{\mathrm{T}}^{1} > 45$ GeV $p_{\mathrm{T}}^{2} > 20$ GeV + ≤ 1 extra jets	2 b-tags $p_{\mathrm{T}}^{1} > 45$ GeV $p_{\mathrm{T}}^{2} > 20$ GeV + 0 extra jets	2 b-tags $p_{\mathrm{T}}^{1} > 45$ GeV $p_{\mathrm{T}}^{2} > 20$ GeV -
Missing E_T	$E_{\mathrm{T}}^{\mathrm{miss}} > 120$ GeV $p_{\mathrm{T}}^{\mathrm{miss}} > 30$ GeV $\Delta\phi(E_{\mathrm{T}}^{\mathrm{miss}}, p_{\mathrm{T}}^{\mathrm{miss}}) < \pi/2$ Min$[\Delta\phi(E_{\mathrm{T}}^{\mathrm{miss}}, \mathrm{jet})] > 1.5$ $\Delta\phi(E_{\mathrm{T}}^{\mathrm{miss}}, b\bar{b}) > 2.8$	-	$E_{\mathrm{T}}^{\mathrm{miss}} < 60$ GeV
Vector Boson	-	$m_{\mathrm{T}}^{W} < 120$ GeV	$83 < m_{\ell\ell} < 99$ GeV

Table 2: Further topological cuts for the three channels in separate p_{T}^{V} intervals.

0-lepton channel					
$E_{\mathrm{T}}^{\mathrm{miss}}$ (GeV)	120-160		160-200		>200
$\Delta R(b,\bar{b})$	0.7-1.9		0.7-1.7		<1.5
1-lepton channel					
p_{T}^{W} (GeV)	0-50	50-100	100-150	150-200	>200
$\Delta R(b,\bar{b})$	>0.7			0.7-1.6	<1.4
$E_{\mathrm{T}}^{\mathrm{miss}}$ (GeV)	> 25				> 50
m_{T}^{W}(GeV)	> 40			-	
2-lepton channel					
p_{T}^{Z}(GeV)	0-50	50-100	100-150	150-200	>200
$\Delta R(b,\bar{b})$	>0.7			0.7-1.8	<1.6

are taken from simulation.

Control regions are used to obtain the normalisation of the top background from data in the 1- and 2-lepton channels. In the 1-lepton channel the control region is defined by requiring an additional jet, and for the 2-lepton channel by inverting the requirements on $m_{\ell\ell}$ and $E_{\mathrm{T}}^{\mathrm{miss}}$. Here top refers to the sum of $t\bar{t}$ and single top production, which are treated together. The ratio of $t\bar{t}$ to single top production is taken from the theory prediction and a systematic uncertainty is assigned to it.

Control distributions to study the V+ jets background are made by relaxing the requirement on 2 b-tagged jets. Events are categorised according to the number of b-tagged jets to define the signal and control regions. The 0-tag and 1-tag control regions contain exactly 0 or 1 b-tagged jets. The pre-tag control region is the sum of the 0-tag, 1-tag control regions and 2-tag signal region. Studying these distributions using the high statistics of the $\sqrt{s}$ = 8 TeV dataset permits more detailed studies of the modelling of several crucial backgrounds. These studies have revealed limitations in the modelling of certain distributions by the Monte Carlo simulation particularly in terms of the vector boson p_{T} spectra. For a number of backgrounds the vector boson p_{T} distribution of the data falls more rapidly than predicted by the Monte Carlo. Therefore corrections were obtained from the high statistics pre-tag regions for both W and Z+jets. The corrections are applied to the V+jets of all flavours and checked in the 1 tag region. The result of this correction is to soften the simulated p_{T}^{V} distribution so that that the fraction of events in the higher p_{T}^{V} bins are reduced by ~5-10%. A similar ~15% correction is derived for the top background using both the 3-jet and an additional 4-jet control region from the 1-lepton analysis. Systematic uncertainties for each correction are included.

The multijet background in each channel is estimated from data. It is found to be $\sim$ 1% in the 0-lepton channel using an 'ABCD method'. In this method, the data are divided into 4 regions based on the variables Min[$\Delta\phi(E_{\mathrm{T}}^{\mathrm{miss}}, \mathrm{jet})$] and $\Delta\phi(E_{\mathrm{T}}^{\mathrm{miss}}, p_{\mathrm{T}}^{\mathrm{miss}})$, such that three of the regions are dominated by background. The background in the signal region, defined by high Min[$\Delta\phi(E_{\mathrm{T}}^{\mathrm{miss}}, \mathrm{jet})$] and low $\Delta\phi(E_{\mathrm{T}}^{\mathrm{miss}}, p_{\mathrm{T}}^{\mathrm{miss}})$ is then evaluated under the assumption that the variables are not correlated. In the 1-lepton channel a multijet template is obtained by reversing the track isolation requirements on the leptons and subtracting W, Z and top contaminations. The template for the other background processes is taken from the Monte Carlo simulation. The normalisations of the two templates are allowed to float in a fit to the $E_{\mathrm{T}}^{\mathrm{miss}}$ distribution. The multijet background in the 1-lepton channel ranges from 23% to 2% of the total background rapidly decreasing with p_{T}^{W}. A shape template for the multijet background in the 2-lepton channel is estimated from data by inverting the isolation and relaxing the lepton quality requirements. It is normalised to the signal selection using the $m_{\ell\ell}$ distribution. The multijet background is found to be < 1% for the 2-lepton channel.

The normalisations of the $V + c$ and V+light backgrounds are determined by a maximum likelihood fit to control and signal regions in the 1- and 2-lepton channels. Events containing 0, 1 and 2 b-tagged jet and the top control regions of each channel are used. This flavour fit exploits the fact that the b-tagging has very different efficiencies for b, c and light jets, such that the flavour composition varies significantly with the number of b-tagged jets. The normalisations of Z+light, $Z + c$, $Z + b$, W+light, $W + c$, $W + b$ and top are allowed to float in the fit.

The distributions of the control and signal regions for each of the three channels after having been normalised by the result of the flavour fit are shown in Figs. 1, 2 and 3 for the $\sqrt{s}$ = 8 TeV data. As the pre-tag and 0-tag samples are almost identical, only the former are shown. The 1-lepton case (Fig. 2) is the simplest to fit because the pre-tag region has a high purity of W+light, the 1-tag region a high purity of W+c and the 2-tag region a high purity of W+b. This means that the constraint on the W+light background comes mainly from the 0-tag region, the constraint on W+c from the 1-tag region and the W+b from the signal region. The 2-lepton case is more complex because the relative fraction of events with b-jets to events with c-jets is higher, such that there is already a significant contribution from processes with real b-jets in the 1-tag region. The 0-lepton channel is a mix of the two, with

approximately equal contribution in each control region from W and Z, with the same flavour mixes as the 1- and 2-lepton channels, respectively.

The flavour fit results for $V + c$ and $V+$ light jets are shown in Table 3 for both the $\sqrt{s} = 7$ TeV and $\sqrt{s} = 8$ TeV datasets as scale factors with respect to the predicted Monte Carlo cross sections. Consistent scale factors are obtained for both datasets except for $Z + c$ production. This is expected, because the two samples were generated using different programs, ALPGEN and SHERPA. Some of the $Z + c$ events arise from charm production in the parton shower of Z+light parton events. However, in the ALPGEN samples used for the $\sqrt{s} = 7$ TeV datasets, the limited statistics in the Z+light sample meant that the contribution from charm from the shower was suppressed to improve the statistical precision from the MC. As a result, the larger scale factor from the flavour fit compensates for this missing charm component. Due to a possible signal contamination and the impact of systematics on the scale factors, the results of this fit are not used to determine the final top and $V + b$ background normalisations. These normalisations are determined later in the fit used to calculate the limits as described in section 7.

The systematic uncertainties on the flavour fit scale factors are determined by propagating the changes from all systematic uncertainties as described in Section 6 into the flavour fit and obtaining the variations in the scale factors. Using this method, the uncertainty on the $Z + c$ and $W + c$ backgrounds is conservatively determined to be 30%, which is included in the final fit.

Table 3: Rescaling factors obtained from a fit to the data for the $V+$ light and c-jet backgrounds. The error includes statistical and systematic uncertainties. The numbers for $Z + c$ are not expected to match between years; see text for details.

	$\sqrt{s} = 7$ TeV	$\sqrt{s} = 8$ TeV
$Z + c$	1.99 ± 0.51	0.71 ± 0.23
$Z+$ light	0.91 ± 0.12	0.98 ± 0.11
$W + c$	1.04 ± 0.23	1.04 ± 0.24
$W+$ light	1.03 ± 0.08	1.01 ± 0.14

6 Systematic Uncertainties

6.1 Theoretical Uncertainties

The WH and ZH signals are normalised to the inclusive cross sections from Refs. [24, 41] evaluated at $\sqrt{s} = 7$ and 8 TeV. For both WH and ZH signals these are the next-to-next-to leading order (NNLO) QCD and NLO EW parton-level computations. The cross sections include inclusive electroweak correction factors Δ_{EW} that are integrated over the entire VH phase space. The relative uncertainty on the Higgs boson branching ratio to $b\bar{b}$ increases with mass and is 3.3% for $m_H = 125$ GeV. The uncertainties on the inclusive cross sections include uncertainties on the renormalisation/factorisation scales and PDF. These uncertainties are considered as correlated between WH and ZH production (the initial state is dominantly $q\bar{q}$ in both cases).

Fully differential NLO EW+QCD cross sections have been calculated, and the effects of the NLO EW corrections have a strong dependence on the vector boson p_{T}. The corrections for the differential EW cross sections, δ_{EW}, are therefore applied as a function of p_{T}^V on the LO WH and ZH signals generated with PYTHIA8, after rescaling to the inclusive NNLO QCD + EW cross section.

Most backgrounds are normalised to data, but the analysis relies on Monte Carlo predictions in certain key areas. Uncertainties for V+jets are estimated for the modelling of the shape of the $m_{b\bar{b}}$ and p_{T}^V distributions. The sidebands of the $m_{b\bar{b}}$ distribution ($m_{b\bar{b}} < 80$ GeV or $m_{b\bar{b}} > 140$ GeV) for the

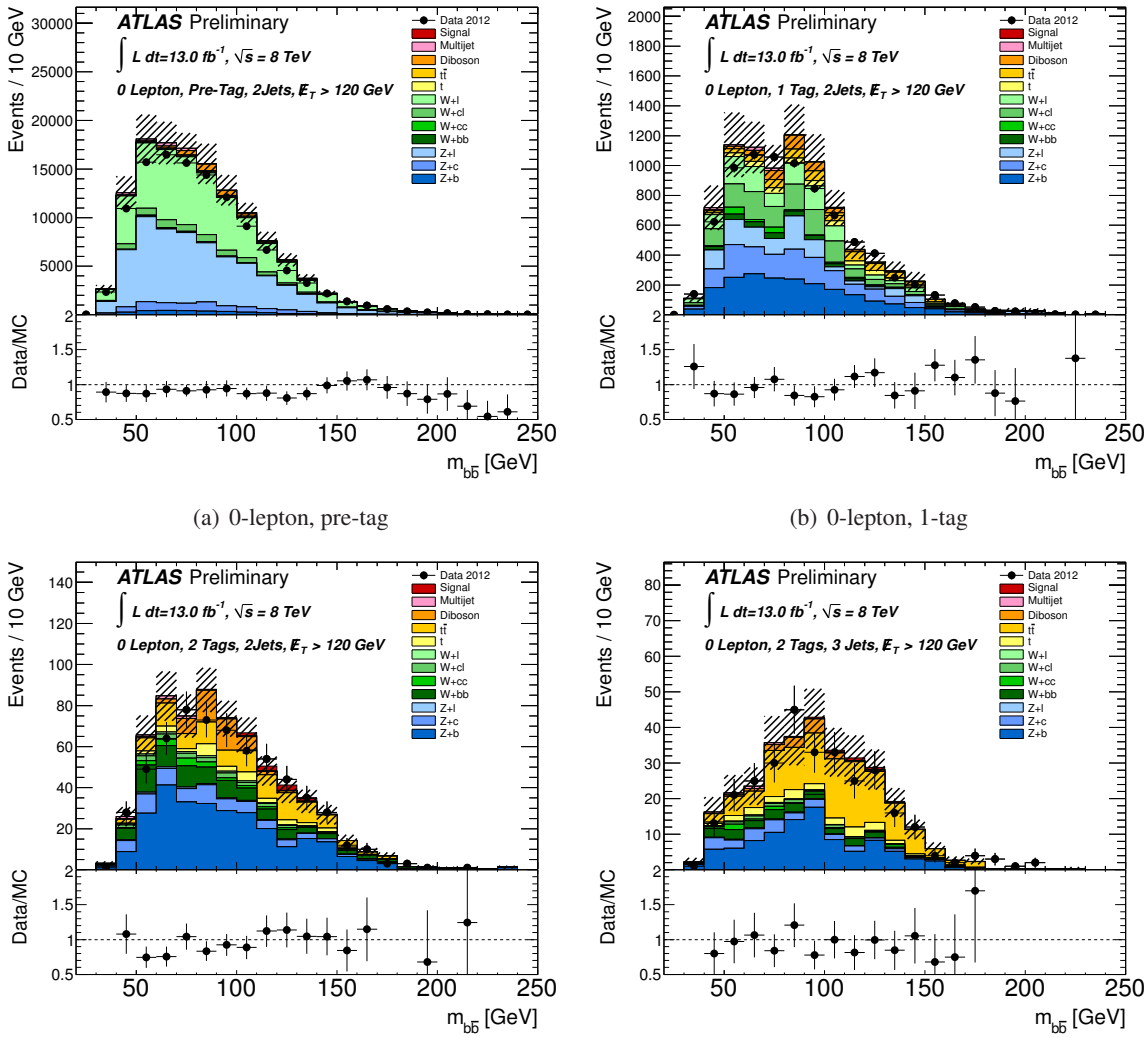

(a) 0-lepton, pre-tag

(b) 0-lepton, 1-tag

(c) 0-lepton, 2-tag, 2-jets

(d) 0-lepton, 2-tag, 3 jets

Figure 1: The $m_{b\bar{b}}$ distributions for the signal and control regions (bottom and top plots respectively) for the 0-lepton selection integrated over the bins of p_{T}^{V}. The error bands indicate the size of the combined statistical and systematic uncertainty before the profile likelihood fit. See text for details of the definition of the control regions.

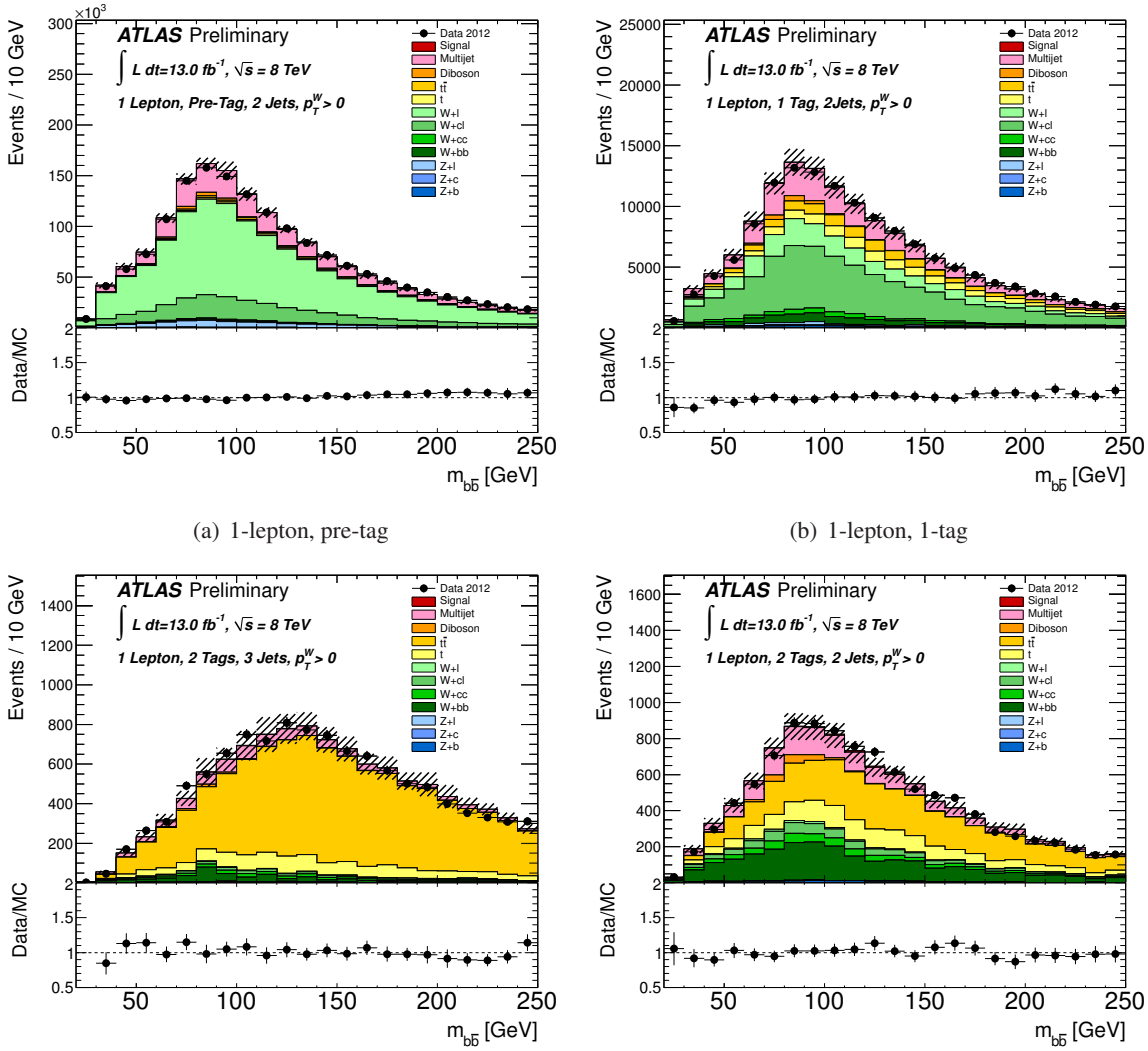

(a) 1-lepton, pre-tag

(b) 1-lepton, 1-tag

(c) 1-lepton, 2-tag, 3-jets

(d) 1-lepton, 2-tag

Figure 2: The $m_{b\bar{b}}$ distributions for the signal (bottom right) and control (top and bottom left) regions for the 1-lepton selection integrated over the bins of p_{T}^{V}. The error bands indicate the size of the combined statistical and systematic uncertainty before the profile likelihood fit. See text for details of the definition of the control regions.

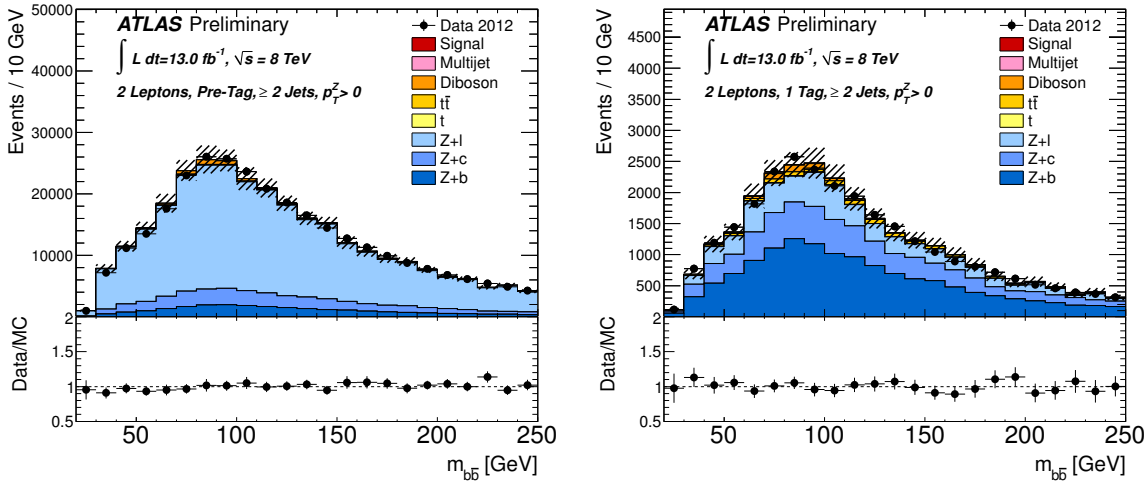

(a) 2-lepton, pre-tag

(b) 2-lepton, 1-tag

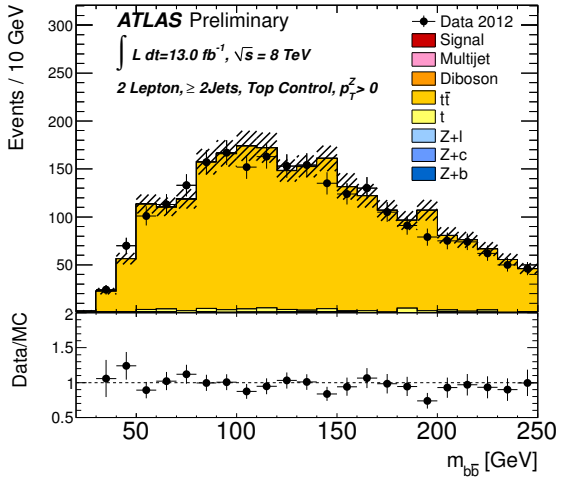

(c) 2-lepton, top control

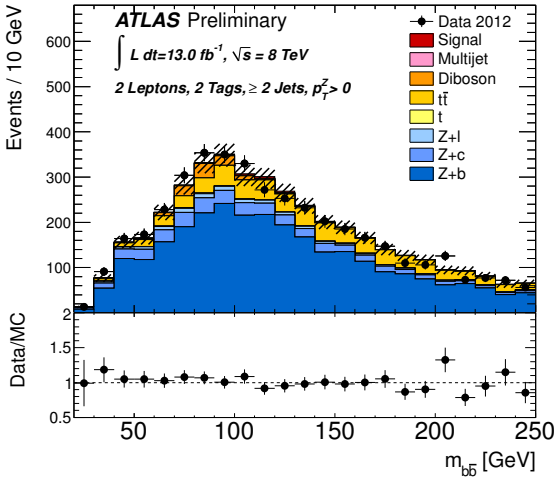

(d) 2-lepton, 2-tag

Figure 3: The $m_{b\bar{b}}$ distributions for the signal (bottom right) and control (top and bottom left) regions for the 2-lepton selection integrated over the bins of p_{T}^{V}. The error bands indicate the size of the combined statistical and systematic uncertainty before the profile likelihood fit. See text for details of the definition of the control regions.

2-lepton category are mostly $Z + b$ events, therefore these uncertainties are estimated by comparing data to simulation in those sidebands. There is no comparably pure control region for $W + b$, therefore those modelling uncertainties are estimated from comparisons between different Monte Carlo generators. The uncertainty on the shape of the $m_{b\bar{b}}$ distribution is parameterised as a linear distortion, correlated between the different p_{T}^V bins. The p_{T}^V uncertainty is treated as five uncorrelated uncertainties in the range between 5 and 10%, one for each p_{T}^V bin. Both are treated separately for W and Z bosons, but correlated between the different lepton channels. The systematic uncertainty applied for the top p_{T}^V correction is again applied in five bins with no correlation between the bins.

Uncertainties on the relative composition of the backgrounds are applied. These are an uncertainty of 15% on the ratio of $t\bar{t}$ to single top, 30% on the $W + c$ normalisation and 30% on the $Z + c$ normalisation. There is a theoretical uncertainty of 11% on the diboson cross section.

6.2 Experimental Uncertainties

Experimental uncertainties affect both the expected signal and background yields and are associated with the reconstruction efficiency and the energy or momentum scale and resolution of the reconstructed objects in the event. The most significant contributions are from the b-tagging efficiencies and the jet energy scale.

The b-tagging performance for b, c and light jets is measured from data [36–38]. These calibrations are applied as MC-to-data scale factors, which depend on the kinematics of the jet. The uncertainties on the scale factors are the statistical and systematic uncertainties of the calibrations. The uncertainties for b-jets are applied as six uncorrelated components for six jet p_{T} bins. The uncertainties on c- and light-jets, which the analysis is less sensitive to, are each accounted for by a single nuisance parameter in the fit used to derive the final limits. The addition of $t\bar{t}$ events for calibration [39] contributes significantly to the accuracy of the measurement.

The jet energy scale uncertainty is separated into eight uncorrelated components. The uncertainty on the jet energy resolution is also applied. In addition to the propagation of the uncertainties on the individual physics objects to the missing transverse energy, uncertainties on the scale and resolution of the so-called soft components, corresponding to energy clusters that have not been associated with other reconstructed physics objects, are applied. A 5% uncertainty on data/MC differences in the modelling of the efficiency of the missing energy trigger is applied for the 0-lepton category.

The normalisation uncertainty on the multijet background is estimated to be 30% for the 1-lepton channel and 100% for the 0- and 2-lepton channels. The uncertainty on the integrated luminosity of 3.9% (3.6%) for $\sqrt{s} = 7$ TeV ($\sqrt{s} = 8$ TeV) is applied to the signal and those backgrounds directly estimated from simulation. A 3% uncertainty on MC modelling of the total number of interactions per bunch crossing is applied to the MC samples.

The impact from uncertainties on the leptons is small, but uncertainties on the trigger and reconstruction efficiency, energy scale and resolution were studied.

The most important systematic uncertainties are summarised in Table 4 and 5 which shows their impact on the total background and signal for respectively for the $\sqrt{s} = 8$ TeV dataset. Similar results are obtained for the $\sqrt{s} = 7$ TeV data.

7 Results

The selection cuts and data analysis procedure were determined without looking at the data in the signal regions. The expected number of signal ($m_H = 125$ GeV) and background events passing the full event selection after the profile likelihood fit are shown for each lepton category, and in bins of p_{T}^V, in Table 6. Also included in the table is the total expected background with its uncertainty. The uncertainty is

Table 4: A summary of the size of the components of the systematic uncertainty on the total estimated background after all cuts for the three channels of the $\sqrt{s} = 8$ TeV analysis. The uncertainties are shown as a percentage and grouped together into broad categories and are averaged over all p_{T}^{V} bins in each category. The total error is worked out by adding the individual components together in quadrature in each p_{T}^{V} bin and then averaging.

Uncertainty [%]	0 lepton	1 lepton	2 leptons
b-tagging	6.5	6.0	6.9
c-tagging	7.3	6.4	3.6
light tagging	2.1	2.2	2.8
Jet/Pile-up/$E_{\mathrm{T}}^{\mathrm{miss}}$	20	7.0	5.4
Lepton	0.0	2.1	1.8
Top modelling	2.7	4.1	0.5
W modelling	1.8	5.4	0.0
Z modelling	2.8	0.1	4.7
Diboson	0.8	0.3	0.5
Multijet	0.6	2.6	0.0
Luminosity	3.6	3.6	3.6
Statistical	8.3	3.6	6.6
Total	25	15	14

Table 5: A summary of the size of the components of the systematic uncertainty on the signal with $m_H = 125$ GeV for the three channels of the $\sqrt{s} = 8$ TeV analysis. The dominant signal is shown for the 1 lepton and 2 lepton channels, while for the 0 lepton channel both ZH and WH signals are listed. The uncertainties are shown as a percentage, grouped together into broad categories and are calculated by summing in quadrature within each p_{T}^{V} bin and then averaging over all p_{T}^{V} bins in a channel.

Uncertainty [%]	0 lepton		1 lepton	2 leptons
	ZH	WH	WH	ZH
b-tagging	8.9	9.0	8.8	8.6
Jet/Pile-up/$E_{\mathrm{T}}^{\mathrm{miss}}$	19	25	6.7	4.2
Lepton	0.0	0.0	2.1	1.8
$H \to bb$ BR	3.3	3.3	3.3	3.3
VH p_T-dependence	5.3	8.1	7.6	5.0
VH theory PDF	3.5	3.5	3.5	3.5
VH theory scale	1.6	0.4	0.4	1.6
Statistical	4.9	18	4.1	2.6
Luminosity	3.6	3.6	3.6	3.6
Total	24	34	16	13

Table 6: The expected numbers of signal and background events for the $\sqrt{s} = 8$ TeV data after the profile likelihood fit, as well as the observed number of events, are shown. The expected number of signal events are shown for WH and ZH production separately for $m_H = 125$ GeV. The quoted error on the total background represents one standard deviation of the profiled nuisance parameters incorporating both the systematic and statistical uncertainties.

	0-lepton, 2 jet			0-lepton, 3 jet			1-lepton					2-lepton				
Bin	$E_{\mathrm{T}}^{\mathrm{miss}}$ [GeV]						p_{T}^{W} [GeV]					p_{T}^{Z}[GeV]				
	120-160	160-200	>200	120-160	160-200	>200	0-50	50-100	100-150	150-200	> 200	0-50	50-100	100-150	150-200	>200
ZH	2.9	2.1	2.6	0.8	0.8	1.1	0.3	0.4	0.1	0.0	0.0	4.7	6.8	4.0	1.5	1.4
WH	0.8	0.4	0.4	0.2	0.2	0.2	10.6	12.9	7.5	3.6	3.6	0.0	0.0	0.0	0.0	0.0
Top	89	25	8	92	25	10	1440	2276	1120	147	43	230	310	84	3	0
$W + c$,light	30	10	5	9	3	2	580	585	209	36	17	0	0	0	0	0
$W + b$	35	13	13	8	3	2	770	778	288	77	64	0	0	0	0	0
$Z + c$,light	35	14	14	8	5	8	17	17	4	1	0	201	230	91	12	15
$Z + b$	144	51	43	41	22	16	50	63	13	5	1	1010	1180	469	75	51
Diboson	23	11	10	4	4	3	53	59	23	13	7	37	39	16	6	4
Multijet	3	1	1	1	1	0	890	522	68	14	3	12	3	0	0	0
Total Bkg.	361	127	98	164	63	42	3810	4310	1730	297	138	1500	1770	665	97	72
	± 29	± 11	± 12	± 13	± 8	± 5	± 150	± 86	± 90	± 27	± 14	± 90	± 110	± 47	± 12	± 12
Data	342	131	90	175	65	32	3821	4301	1697	297	132	1485	1773	657	100	69

reduced compared with table 4 due to the normalisation procedure described below. The numbers of observed events in data are shown in the last row. After all selection criteria, the dominant backgrounds are $Z + b$ production for the 2-lepton category, $W + b$ and top production for the 1-lepton category, and all three contribute significantly for the 0-lepton category. The signal to background ratio improves in each channel with increasing p_{T}^{V}. The total expected background and its uncertainty is included. The uncertainty is reduced compared with Table 4 due to the normalisation procedure described below.

The statistical analysis of the data employs a binned likelihood function $\mathcal{L}(\mu, \theta)$ constructed as the product of Poisson probability terms for each category. The categories that enter the profile likelihood fit are the 16 individual 2 b-tag signal regions and the top control regions for the 1- and 2-lepton channels. A signal strength parameter, μ, multiplies the expected Standard Model Higgs boson production cross section in each bin. The dependence of the signal and background predictions on the systematic uncertainties is described by nuisance parameters, θ, which are parametrised by Gaussian or log-normal priors. The expected number of signal and background events in each bin are functions of θ. The parametrisation is chosen such that the rates in each category are log-normally distributed for a normally distributed θ. The test statistic q_μ is then constructed according to the profile likelihood: $q_\mu = 2\ln(\mathcal{L}(\mu, \hat{\theta}_\mu)/\mathcal{L}(\hat{\mu}, \hat{\theta}))$, where $\hat{\mu}$ and $\hat{\theta}$ are the parameters that maximise the likelihood (with the constraint $0 \leq \hat{\mu} \leq \mu$), and $\hat{\theta}_\mu$ are the nuisance parameter values that maximise the likelihood for a given μ. This test statistic is used to measure the compatibility of the background only model with the observed data and for exclusion intervals derived with the CL_s method [42, 43]. The normalisation of the top, $Z + b$ and $W + b$ backgrounds are allowed to float freely in the fit. The other backgrounds are constrained within their errors as described in section 5. The resulting scale factors from the fit are shown in table 7 for both $\sqrt{s} = 7$ TeV and $\sqrt{s} = 8$ TeV.

Diboson production with a Z boson decaying to a pair of b-quarks and produced with either a W or Z boson has a very similar signature but with lower p_{T}^{Z} and $m_{b\bar{b}}$ peaking at lower values and with a cross section ∼5 times larger than Higgs boson associated production. Therefore a separate fit was made as a validation of the analysis procedure. This fit is performed as described above, except that

Table 7: Rescaling factors obtained from the fit to the data for the $V + b$ and top backgrounds. The error includes statistical and systematic uncertainties.

	$\sqrt{s} = 7$ TeV	$\sqrt{s} = 8$ TeV
Top	1.10 ± 0.14	1.29 ± 0.16
$Z + b$	1.22 ± 0.20	1.11 ± 0.15
$W + b$	1.19 ± 0.23	0.79 ± 0.20

there is no separation in p_{T}^{V} bins. In the fit the normalisation of the diboson contributions is allowed to vary with a multiplicative scale μ_D with respect to the Standard Model expectation. A Standard Model Higgs boson with $m_H = 125$ GeV is included as a background. Figure 4 shows the distribution in data after subtracting all backgrounds except the diboson contributions. The backgrounds are evaluated after the results of the profile likelihood fit. An excess in the data compared to the background is observed and this excess is located at the expected mass for the vector boson signal. After combining the three channels and including all systematic uncertainties we measure $\mu_D = 1.09 \pm 0.20(\mathrm{stat.}) \pm 0.22(\mathrm{syst.})$. This corresponds to a significance of 4.0 σ and agrees with the Standard Model expectation of $\mu_D = 1$.

The profile likelihood fit with the Higgs boson signal strength floating is then performed with the diboson contribution fixed to its Standard Model expectation, constrained within an uncertainty of 11%, as discussed above.

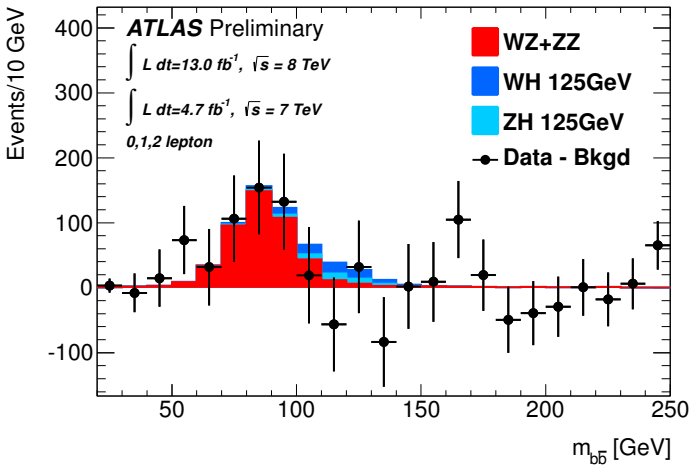

Figure 4: The $m_{b\bar{b}}$ distribution in data after subtraction of all backgrounds except diboson processes including SM Higgs boson from WH and ZH associated production. The MC backgrounds are normalised according to the results of the global fit. Only statistical uncertainties are shown.

Figures 5, 6 and 7 show the $m_{b\bar{b}}$ distribution in $\sqrt{s} = 8$ TeV data after all selection criteria have been applied for each category. The dashed bands indicate the size of the combination of the statistical and systematic uncertainties on the background processes after the likelihood fit. Agreement between data and background is observed within the systematic uncertainties. The corresponding distributions for $\sqrt{s} = 7$ TeV are shown in Figs. 16, 17 and 18 in the supporting material.

Figure 8 shows the results for the 95% confidence level (CL) exclusion limits on the Higgs boson production cross section in the mass range 110-130 GeV. The expected limits range from 1.5 to 3 times the SM expectation over the full mass range for the $\sqrt{s} = 8$ TeV dataset alone. The expected limits for

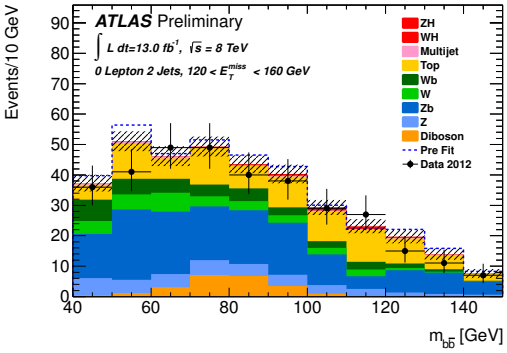

(a) $120 < E_{\mathrm{T}}^{\mathrm{miss}} < 160$ GeV, 2 jets

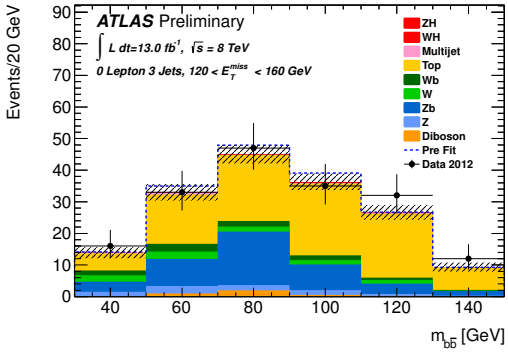

(b) $120 < E_{\mathrm{T}}^{\mathrm{miss}} < 160$ GeV, 3 jets

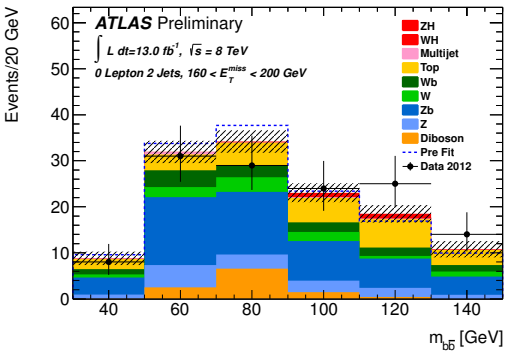

(c) $160 < E_{\mathrm{T}}^{\mathrm{miss}} < 200$ GeV, 2 jets

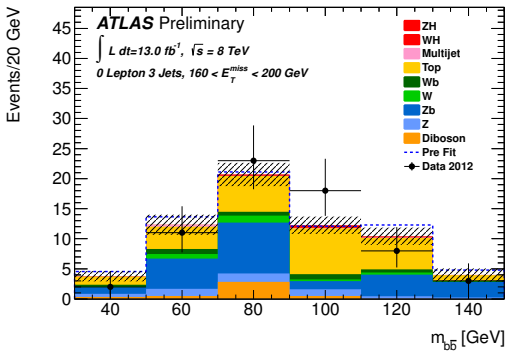

(d) $160 < E_{\mathrm{T}}^{\mathrm{miss}} < 200$ GeV, 3 jets

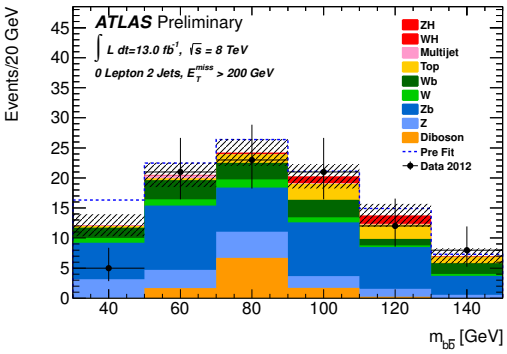

(e) $E_{\mathrm{T}}^{\mathrm{miss}} > 200$ GeV, 2 jets

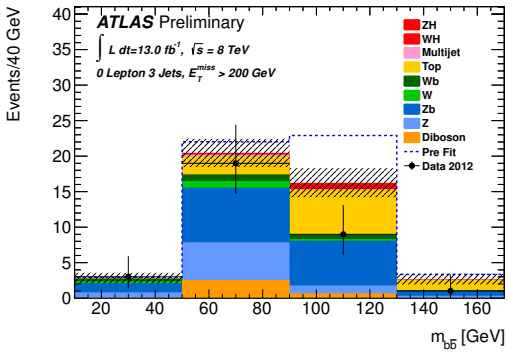

(f) $E_{\mathrm{T}}^{\mathrm{miss}} > 200$ GeV, 3 jets

Figure 5: The $m_{b\bar{b}}$ distribution in data for the six categories of the zero lepton analysis. The signal shown is for $m_H = 125$ GeV. The background from the V+jet process is separated into the $V + b$ and the sum of the $V + c$ and V+light components. The background expectation is shown after the profile likelihood fit (solid) and compared to the predictions from the pre-fit Monte Carlo simulation (dashed). The size of the combined statistical and systematic uncertainty is indicated by the hashed band.

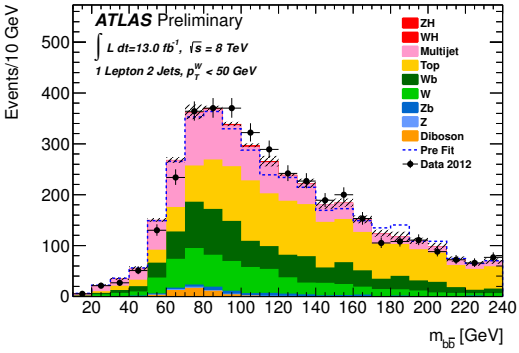

(a) $p_{\mathrm{T}}^{W} < 50$ GeV

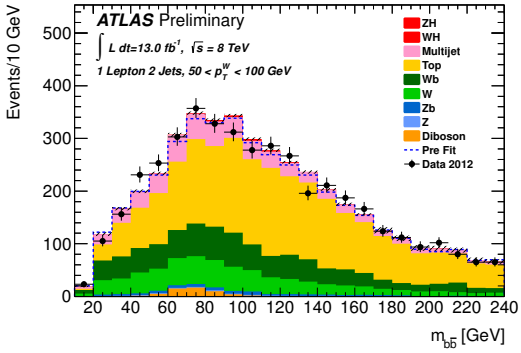

(b) $50 < p_{\mathrm{T}}^{W} < 100$ GeV

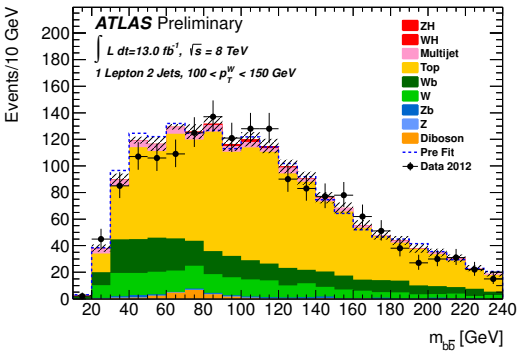

(c) $100 < p_{\mathrm{T}}^{W} < 150$ GeV

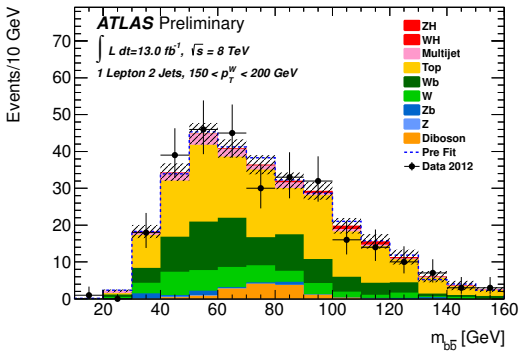

(d) $150 < p_{\mathrm{T}}^{W} < 200$ GeV

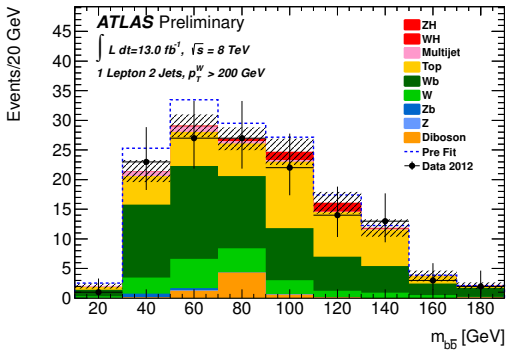

(e) $p_{\mathrm{T}}^{W} > 200$ GeV

Figure 6: The $m_{b\bar{b}}$ distribution in data for the five categories of the one lepton analysis. The signal shown is for $m_H = 125$ GeV. The background from the V+jet process is separated into the $V + b$ and the sum of the $V + c$ and V+light components. The background expectation is shown after the profile likelihood fit (solid) and compared to the predictions from the pre-fit Monte Carlo simulation (dashed). The size of the combined statistical and systematic uncertainty is indicated by the hashed band.

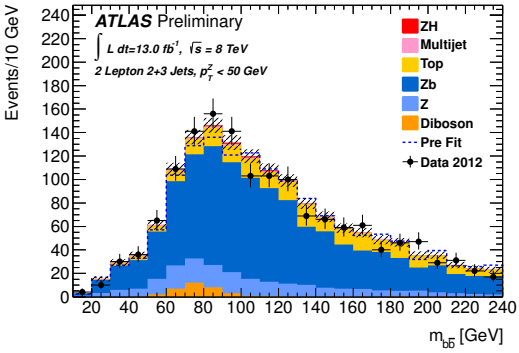

(a) $p_{\mathrm{T}}^{Z} < 50$ GeV

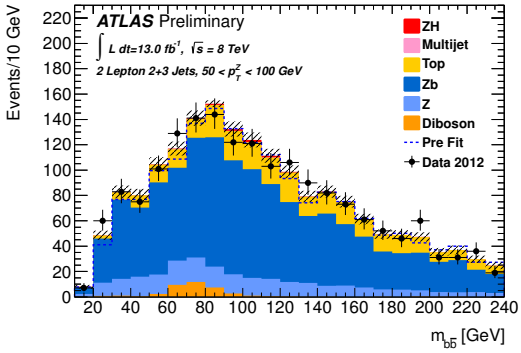

(b) $50 < p_{\mathrm{T}}^{Z} < 100$ GeV

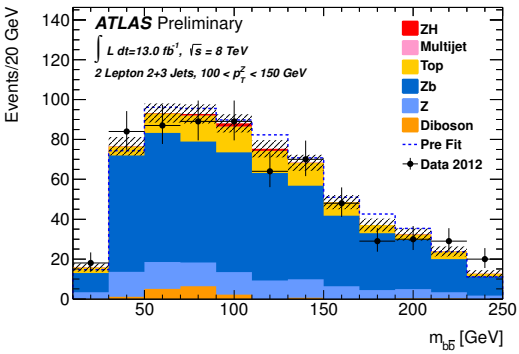

(c) $100 < p_{\mathrm{T}}^{Z} < 150$ GeV

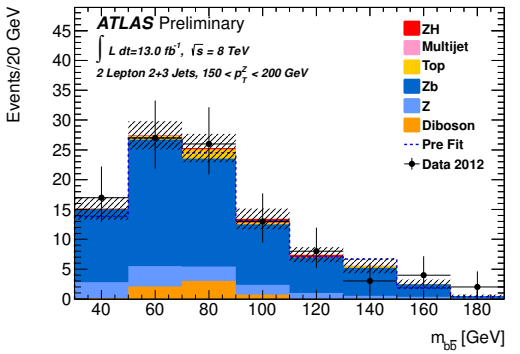

(d) $150 < p_{\mathrm{T}}^{Z} < 200$ GeV

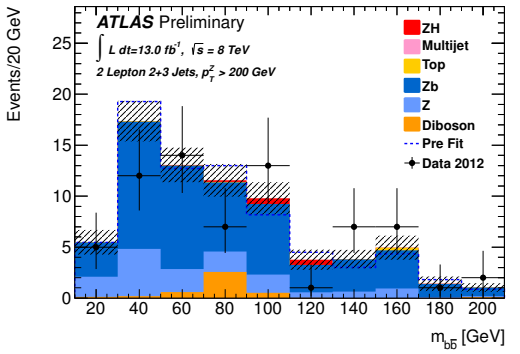

(e) $p_{\mathrm{T}}^{Z} > 200$ GeV

Figure 7: The $m_{b\bar{b}}$ distribution in data for the five categories of the two lepton analysis. The signal shown is for $m_H = 125$ GeV. The background from the V+jet process is separated into the $V + b$ and the sum of the $V + c$ and V+light components. The background expectation is shown after the profile likelihood fit (solid) and compared to the predictions from the pre-fit Monte Carlo simulation (dashed). The size of the combined statistical and systematic uncertainty is indicated by the hashed band.

$m_H = 125$ GeV are 3.3 and 2.5 times the Standard Model expectations for $\sqrt{s} = 7$ TeV and $\sqrt{s} = 8$ TeV, respectively. For the $\sqrt{s} = 7$ TeV data, this presents a significant improvement compared to the expected sensitivity of 4.0 times the Standard Model expectation reported in Ref. [12]. No significant excess is observed. The corresponding observed limits are 1.8 and 3.4 times the Standard Model expectations. This corresponds to a deficit of data events compared to the expectation from background processes of almost 2σ in the $\sqrt{s} = 7$ TeV dataset and an excess of about 1σ in the $\sqrt{s} = 8$ TeV dataset. The observed limit for the combination of the $\sqrt{s} = 7$ TeV and $\sqrt{s} = 8$ TeV datasets is 1.8 times the Standard Model expectation with an expected limit of 1.9 times the Standard Model. A Standard Model Higgs boson with $m_H = 110$ GeV is excluded at the 95% CL.

Figure 9 shows the expected and observed p_0 value in the same mass range. The quantity p_0 represents the probability that a background-only experiment would yield a result that is more signal-like than the observed result. For $m_H = 125$ GeV, the observed p_0 values are 0.97 and 0.17 for the $\sqrt{s} = 7$ TeV and $\sqrt{s} = 8$ TeV datasets, respectively. The expected p_0 values in the presence of a Standard Model Higgs boson are 0.26 and 0.20, respectively. The combination of both datasets yields an observed (expected) p_0 value of 0.64 (0.15). We measure $\mu = -2.7 \pm 1.1(\text{stat.}) \pm 1.1(\text{syst.})$, $\mu = 1.0 \pm 0.9(\text{stat.}) \pm 1.1(\text{syst.})$ and $\mu = -0.4 \pm 0.7(\text{stat.}) \pm 0.8(\text{syst.})$ in the $\sqrt{s} = 7$ TeV, $\sqrt{s} = 8$ TeV and combined datasets.

8 Summary

This note has presented the search by the ATLAS experiment for the Standard Model Higgs boson produced in association with a W or Z boson, where the decay channels $ZH \to \nu\bar{\nu}b\bar{b}$, $WH \to \ell\nu b\bar{b}$ and $ZH \to \ell^+\ell^- b\bar{b}$ have been considered. The dataset corresponds to 4.7 fb^{-1} of LHC pp collision data recorded at $\sqrt{s} = 7$ TeV in the year 2011 and 13.0 fb^{-1} of data recorded at $\sqrt{s} = 8$ TeV in the year 2012. The analyses have been carried out in 16 different categories depending on the number of leptons, number of jets and the transverse momentum of the vector boson candidate. No significant excess is observed. For $m_H = 125$ GeV, the observed (expected) upper limit on the production cross section times the branching ratio is found to be 1.8 (1.9) times the Standard Model prediction for the combined $\sqrt{s} = 7$ TeV and $\sqrt{s} = 8$ TeV datasets.

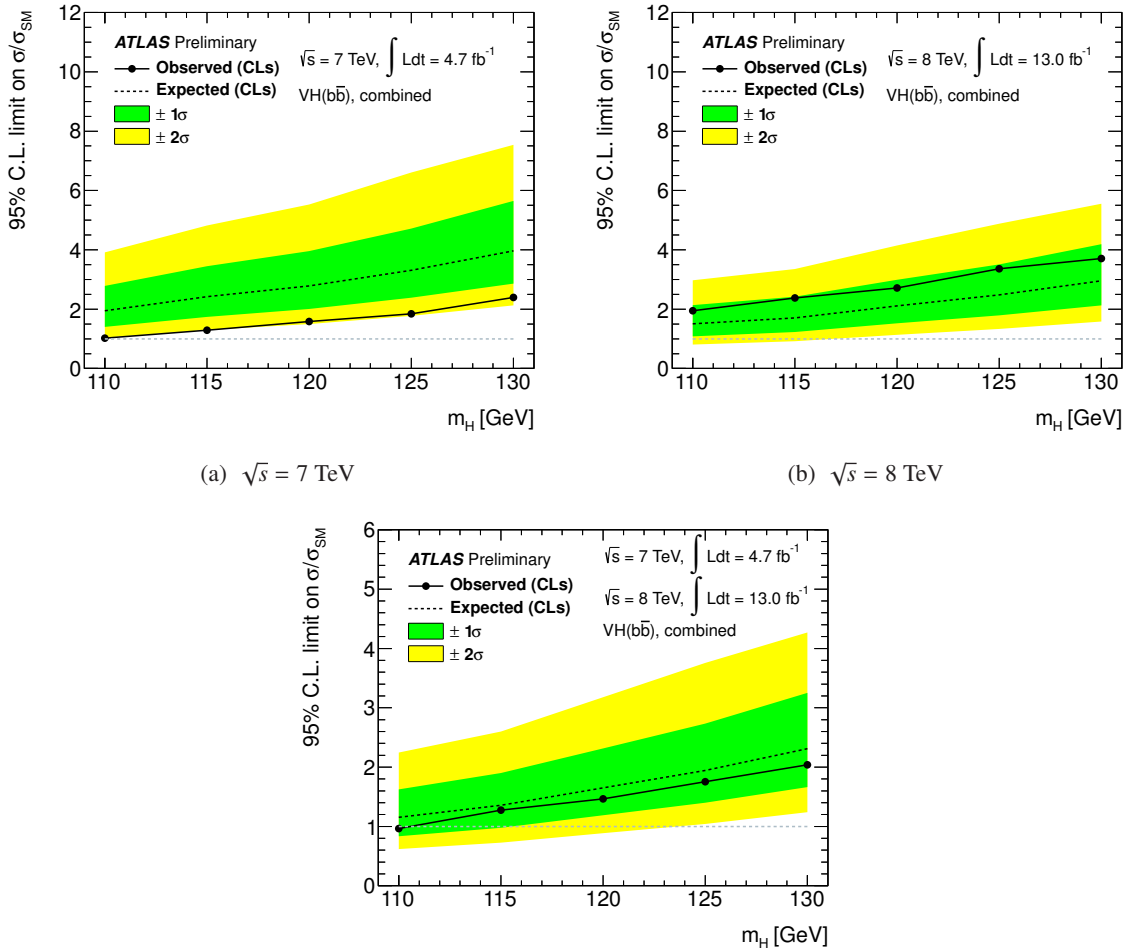

(a) $\sqrt{s} = 7$ TeV

(b) $\sqrt{s} = 8$ TeV

(c) Combination

Figure 8: Expected (dashed) and observed (solid) CL_s limit on the normalised signal strength as a function of m_{H} for all channels for the $\sqrt{s} = 7$ TeV dataset (top left), the $\sqrt{s} = 8$ TeV dataset (top right) and the combination of both datasets (bottom).

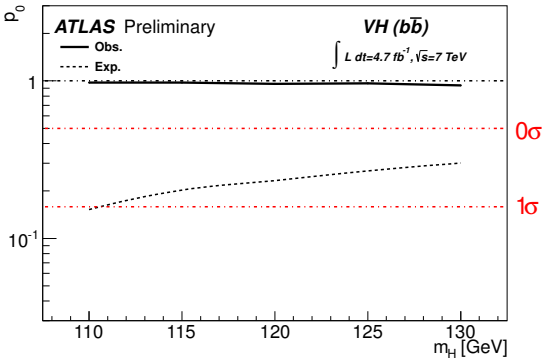

(a) $\sqrt{s} = 7$ TeV

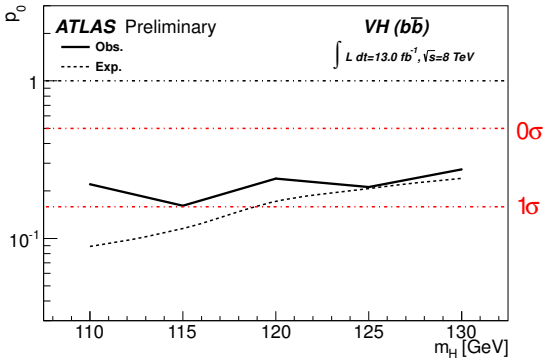

(b) $\sqrt{s} = 8$ TeV

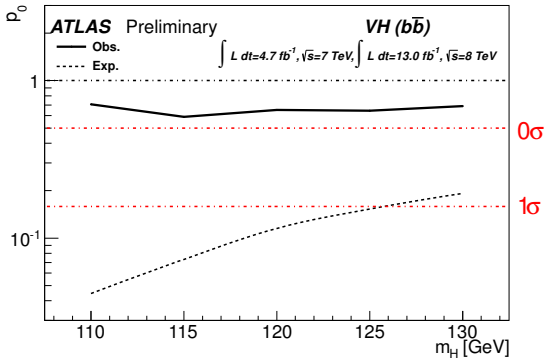

(c) Combination

Figure 9: The observed probability, p_0, in the background-only scenario (solid line) as a function of m_{H}. The dashed line shows the corresponding expectation for the signal+background hypothesis at the given value of m_{H}. The probability is shown separately for the $\sqrt{s} = 7$ TeV (top left), $\sqrt{s} = 8$ TeV (top right) and combined results (bottom).

References

[1] S. L. Glashow, *Partial Symmetries of Weak Interactions*, Nucl. Phys. **22** (1961) 579–588.

[2] S. Weinberg, *A Model of Leptons*, Phys. Rev. Lett. **19** (1967) 1264–1266.

[3] A. Salam, *Weak and electromagnetic interactions*, Proc. of the 8th Nobel Symposium (1969) 367.

[4] F. Englert and R. Brout, *Broken Symmetry and the Mass of Gauge Vector Mesons*, Phys. Rev. Lett. **13** (1964) 321.

[5] P. W. Higgs, *Broken Symmetries and the Masses of Gauge Bosons*, Phys. Rev. Lett. **13** (1964) 508.

[6] P. W. Higgs, *Broken Symmetries, Massless Particles and Gauge Fields*, Phys. Lett. **12** (1964) 132.

[7] G. Guralnik, C. Hagen, and T. Kibble, *Global Conservation Laws and Massless Particles*, Phys. Rev. Lett. **13** (1964) 585.

[8] ATLAS Collaboration, *Observation of a new particle in the search for the Standard Model Higgs boson with the ATLAS detector at the LHC*, Phys.Lett. **B716** (2012) 1–29, arXiv:1207.7214 [hep-ex].

[9] CMS Collaboration, *Observation of a new boson at a mass of 125 GeV with the CMS experiment at the LHC*, Phys.Lett. **B716** (2012) 30–61, arXiv:1207.7235 [hep-ex].

[10] A. Djouadi, J. Kalinowski, and M. Spira, *HDECAY: A program for Higgs boson decays in the Standard Model and its supersymmetric extension*, Comput. Phys. Commun. **108** (1998) 56–74.

[11] CDF Collaboration, D0 Collaboration Collaboration, T. Aaltonen et al., *Evidence for a particle produced in association with weak bosons and decaying to a bottom-antibottom quark pair in Higgs boson searches at the Tevatron*, Phys.Rev.Lett. **109** (2012) 071804, arXiv:1207.6436 [hep-ex].

[12] ATLAS Collaboration, *Search for the Standard Model Higgs boson produced in association with a vector boson and decaying to a b-quark pair with the ATLAS detector*, arXiv:1207.0210 [hep-ex].

[13] ATLAS Collaboration, *Luminosity Determination in pp Collisions at* $\sqrt{s} = 7$ TeV *Using the ATLAS Detector at the LHC*, Eur. Phys. J. C **71** (2011) 1630, arXiv:1101.2185 [hep-ph].

[14] ATLAS Collaboration, *Luminosity Determination in pp Collisions at* $\sqrt{s} = 7$ TeV *using the ATLAS Detector in 2011*, ATLAS-CONF-2011-116 (2011).

[15] ATLAS Collaboration, *The ATLAS Simulation Infrastructure*, Eur. Phys. J **C70** (2010) 823, arXiv:1005.4568 [physics.ins-det].

[16] GEANT4 Collaboration, S. Agostinelli et al., *GEANT4: A Simulation toolkit*, Nucl.Instrum.Meth. **A506** (2003) 250–303.

[17] E. Richter-Was, D. Froidevaux, and L. Poggioli, *ATLFAST 2.0 a fast simulation package for ATLAS*, Tech. Rep. ATL-PHYS-98-131, CERN, Geneva, Nov, 1998.

[18] T. Sjostrand, S. Mrenna, and P. Z. Skands, *A Brief Introduction to PYTHIA 8.1*, Comput.Phys.Commun. **178** (2008) 852–867, arXiv:0710.3820 [hep-ph].

[19] P. M. Nadolsky, H.-L. Lai, Q.-H. Cao, J. Huston, J. Pumplin, et al., *Implications of CTEQ global analysis for collider observables*, Phys.Rev. **D78** (2008) 013004, arXiv:0802.0007 [hep-ph].

[20] ATLAS Collaboration, *ATLAS tunes of PYTHIA6 and PYTHIA8 for MC11*, ATL-PHYS-PUB-2011-009 (2011), http://cdsweb.cern.ch/record/1363300.

[21] T. Sjostrand, S. Mrenna, and P. Z. Skands, PYTHIA *6.4 Physics and Manual*, JHEP **05** (2006) 026, arXiv:hep-ph/0603175.

[22] A. Sherstnev and R. Thorne, *Parton Distributions for LO Generators*, Eur. Phys. J. **C55** (2008) 553–575, arXiv:0711.2473 [hep-ph].

[23] LHC Higgs Cross Section Working Group, S. Dittmaier, C. Mariotti, G. Passarino, and R. Tanaka (Eds.), *Handbook of LHC Higgs Cross Sections: 1. Inclusive Observables*, CERN-2011-002 (CERN, Geneva, 2011), arXiv:1101.0593 [hep-ph].

[24] LHC Higgs Cross Section Working Group, S. Dittmaier, C. Mariotti, G. Passarino, and R. Tanaka (Eds.), *Handbook of LHC Higgs Cross Sections: 2. Differential Distributions*, CERN-2012-002 (CERN, Geneva, 2012), arXiv:1201.3084 [hep-ph].

[25] G. Ferrera, M. Grazzini, and F. Tramontano, *Associated WH production at hadron colliders: a fully exclusive QCD calculation at NNLO*, Phys.Rev.Lett. **107** (2011) 152003, arXiv:1107.1164 [hep-ph].

[26] H.-L. Lai et al., *New parton distributions for collider physics*, **82** (2010) 074024.

[27] G. Corcella et al., *HERWIG 6: an event generator for hadron emission reactions with interfering gluons (including super-symmetric processes*, JHEP **01** (2001) 010.

[28] S. Alioli et al., *NLO Higgs boson production via gluon fusion matched with shower in POWHEG*, JHEP **0904** (2009) 002, arXiv:0812.0578 [hep-ph].

[29] P. Nason and C. Oleari, *NLO Higgs boson production via vector-boson fusion matched with shower in POWHEG*, JHEP **1002** (2010) 037, arXiv:0911.5299 [hep-ph].

[30] C. Oleari and L. Reina, $W^{\pm}b\bar{b}$ *production in POWHEG*, JHEP **1108** (2011) 061, arXiv:1105.4488 [hep-ph].

[31] A. D. Martin et al., *Parton distributions for the LHC*, Eur. Phys. J. **63** (2009) 189, arXiv:0901.0002v3 [hep-ph].

[32] M. L. Mangano et al., ALPGEN*, a generator for hard multi-parton processes in hadronic collisions*, JHEP **07** (2003) 001.

[33] T. Gleisberg et al., *Event generation with SHERPA 1.1*, JHEP **02** (2009) 007, arXiv:0811.4622 [hep-ph].

[34] M. Cacciari, G. P. Salam, and G. Soyez, *The anti-k_t jet clustering algorithm*, JHEP **04** (2008) 063, arXiv:0802.1189 [hep-ph].

[35] ATLAS Collaboration, *Jet energy measurement with the ATLAS detector in proton-proton collisions at* $\sqrt{s} = 7$ *TeV*, arXiv:1112.6426 [hep-ex]. Submitted to Eur. Phys. J. C.

[36] ATLAS Collaboration, *b-jet tagging calibration on c-jets containing D^{*+} mesons*, ATLAS-CONF-2012-039 (2012), https://cdsweb.cern.ch/record/1435193.

[37] ATLAS Collaboration, *Measurement of the Mistag Rate with 5 fb^{-1} of Data Collected by the ATLAS Detector*, ATLAS-CONF-2012-040 (2012), https://cdsweb.cern.ch/record/1435194.

[38] ATLAS Collaboration, *Measurement of the b-tag Efficiency in a Sample of Jets Containing Muons with 5 fb^{-1} of Data from the ATLAS Detector*, ATLAS-CONF-2012-043 (2012), https://cdsweb.cern.ch/record/1435197.

[39] ATLAS Collaboration, *Measuring the b-tag efficiency in a top-pair sample with 4.7 fb-1 of data from the ATLAS detector*, ATLAS-CONF-2012-097 (2012), https://cdsweb.cern.ch/record/1460443.

[40] ATLAS Collaboration, *Performance of Missing Transverse Momentum Reconstruction in Proton-Proton Collisions at $\sqrt{s}$ = 7 TeV with ATLAS*, Eur. Phys. J **C72** (2012) 1844, arXiv:1108.5602 [hep-ex].

[41] S. Dittmaier, M. Kramer, and M. Spira, *Higgs radiation off bottom quarks at the Tevatron and the CERN LHC*, Phys.Rev. **D70** (2004) 074010, arXiv:hep-ph/0309204.

[42] A. L. Read, *Presentation of search results: The CL(s) technique*, J.Phys. **G28** (2002) 2693–2704.

[43] G. Cowan et al., *Asymptotic formulae for likelihood-based tests of new physics*, Eur. Phys. J. **C71** (2011) 1554, arXiv:1007.1727 [physics.data-an].

A Supporting Material for Approval

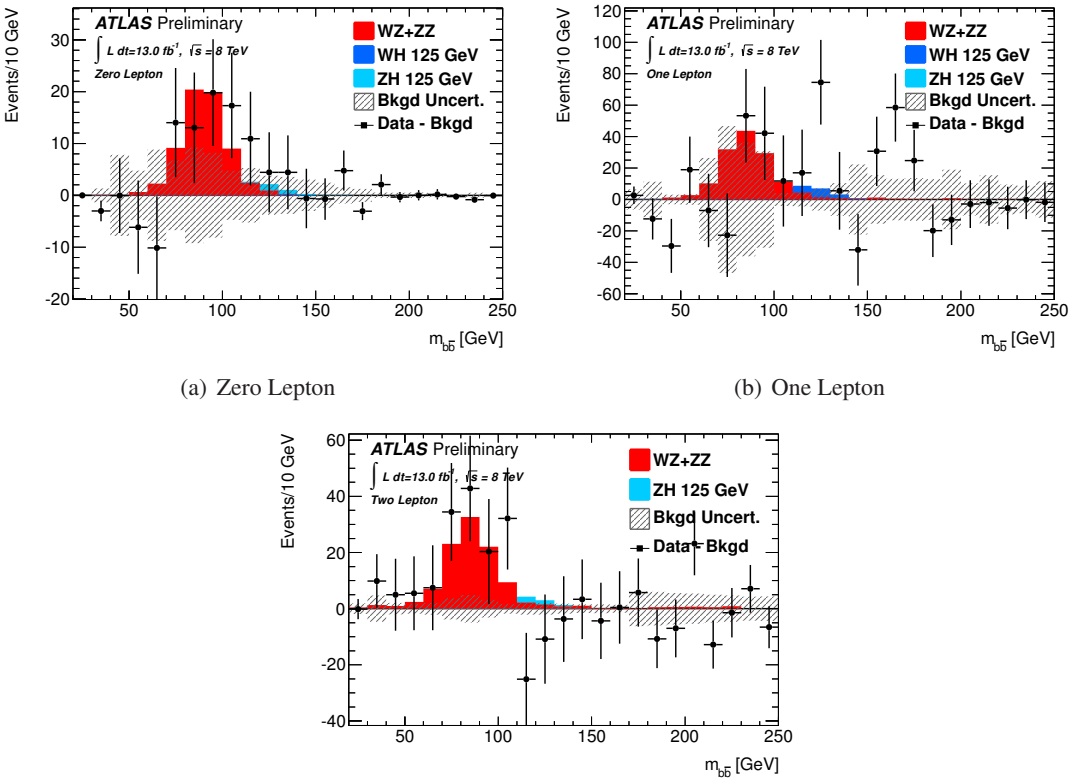

(a) Zero Lepton

(b) One Lepton

(c) Two Lepton

Figure 10: The $m_{b\bar{b}}$ distribution in data after subtraction of all backgrounds except diboson processes including SM Higgs from WH and ZH associated production for the zero, one and two lepton analyses at $\sqrt{s} = 8$ TeV. The distribution is shown after the statistical treatment has been performed. The MC backgrounds are normalized according to the results of the global fit. The systematics uncertainties after the profile likelihood fit are indicated by the dashed band.

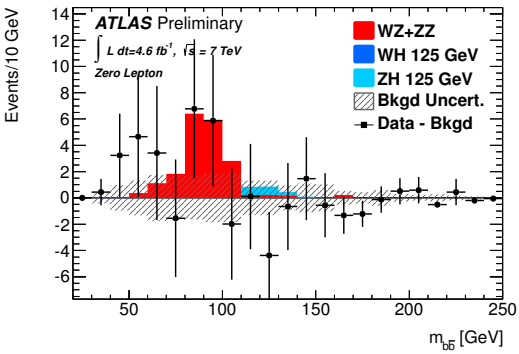

(a) Zero Lepton

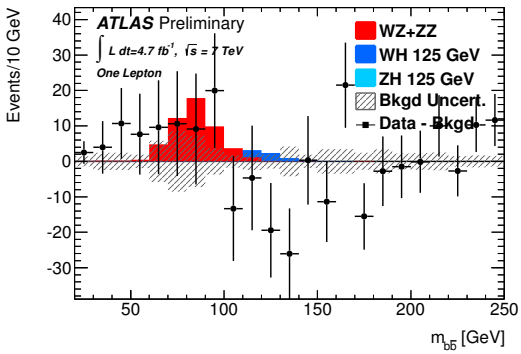

(b) One Lepton

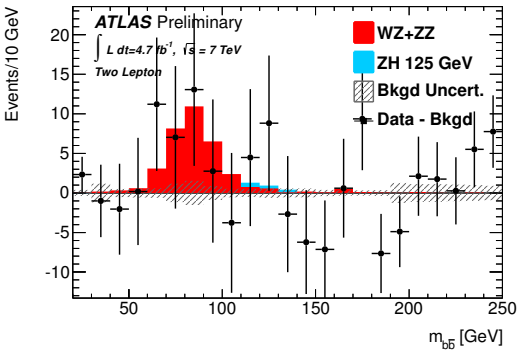

(c) Two Lepton

Figure 11: The $m_{b\bar{b}}$ distribution in data with all estimated backgrounds except diboson production subtracted, overlaid with the prediction from simulation for WZ and ZZ production for the zero, one and two lepton analyses at $\sqrt{s}$ = 7 TeV. The distribution is shown after the statistical treatment has been performed, with the backgrounds normalised by the output of the fit. The systematics uncertainties after the profile likelihood fit are indicated by the dashed band.

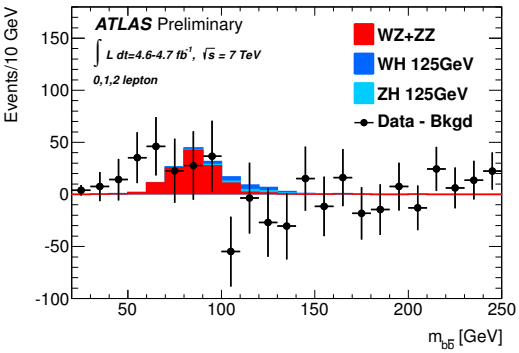

(a) $\sqrt{s}$ = 7 TeV

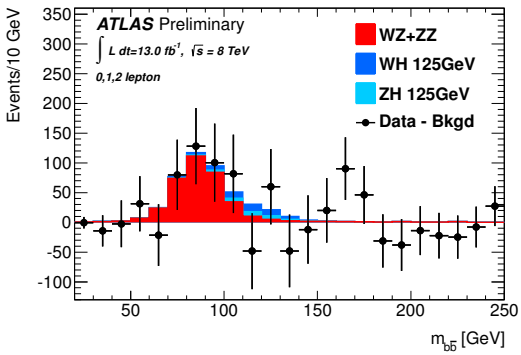

(b) $\sqrt{s}$ = 8 TeV

Figure 12: The $m_{b\bar{b}}$ distribution in data after subtraction of all backgrounds except diboson processes including SM Higgs from WH and ZH associated production for the combined lepton channels at $\sqrt{s}$ = 7 TeV and $\sqrt{s}$ = 8 TeV. The distribution is shown after the statistical treatment has been performed. The MC backgrounds are normalized according to the results of the global fit. Only statistical uncertainties are shown.

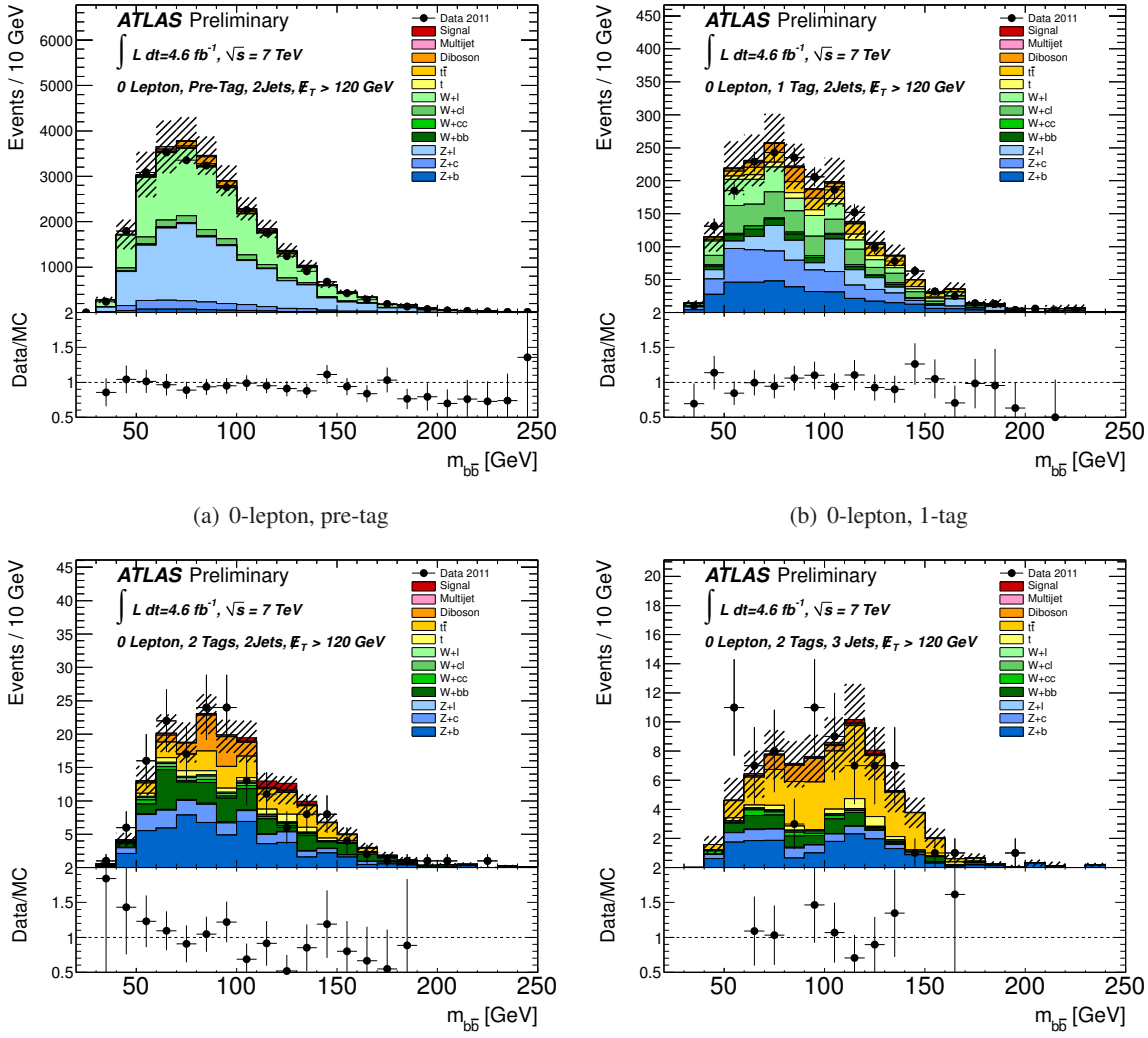

(a) 0-lepton, pre-tag

(b) 0-lepton, 1-tag

(c) 0-lepton, 2-tag, 2-jets

(d) 0-lepton, 2-tag, 3 jets

Figure 13: The control and signal regions for the 0, 1 and 2-lepton selection integrated over the bins of p_{T}^{V} at $\sqrt{s} = 7$ TeV. The error bands indicate the size of the combined statistical and systematic uncertainty before the profile likelihood fit. See text for the precise definition of the control regions.

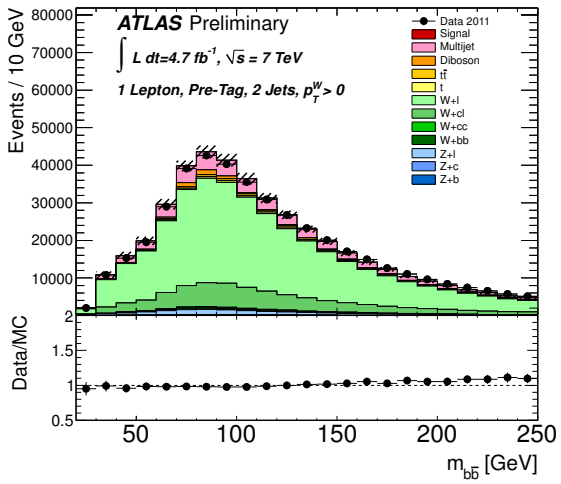

(a) 1-lepton, pre-tag

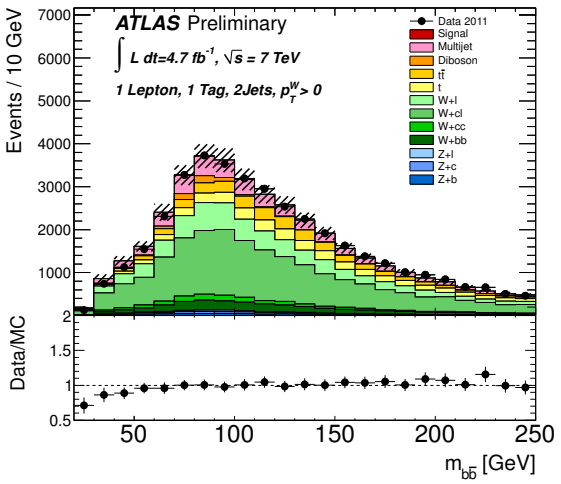

(b) 1-lepton, 1-tag

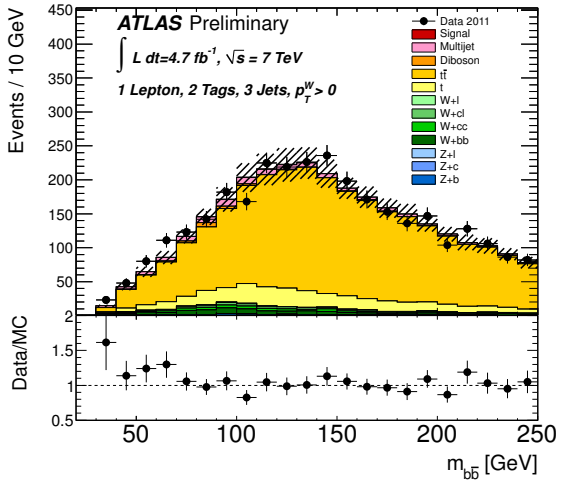

(c) 1-lepton, 2-tag, 3-jets

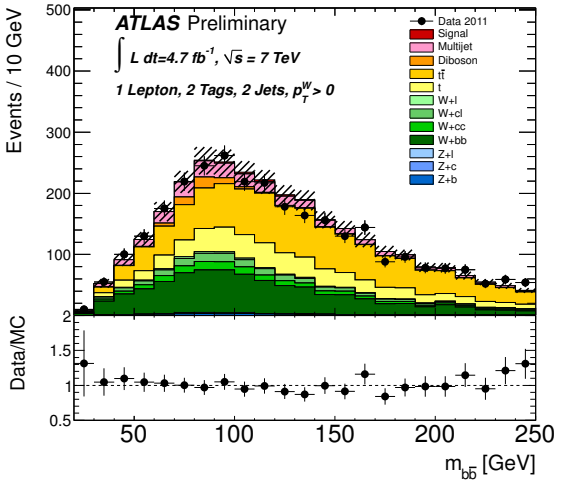

(d) 1-lepton, 2-tag

Figure 14: The control and signal regions for the 0, 1 and 2-lepton selection integrated over the bins of p_{T}^{V} at $\sqrt{s} = 7$ TeV. The error bands indicate the size of the combined statistical and systematic uncertainty before the profile likelihood fit. See text for the precise definition of the control regions.

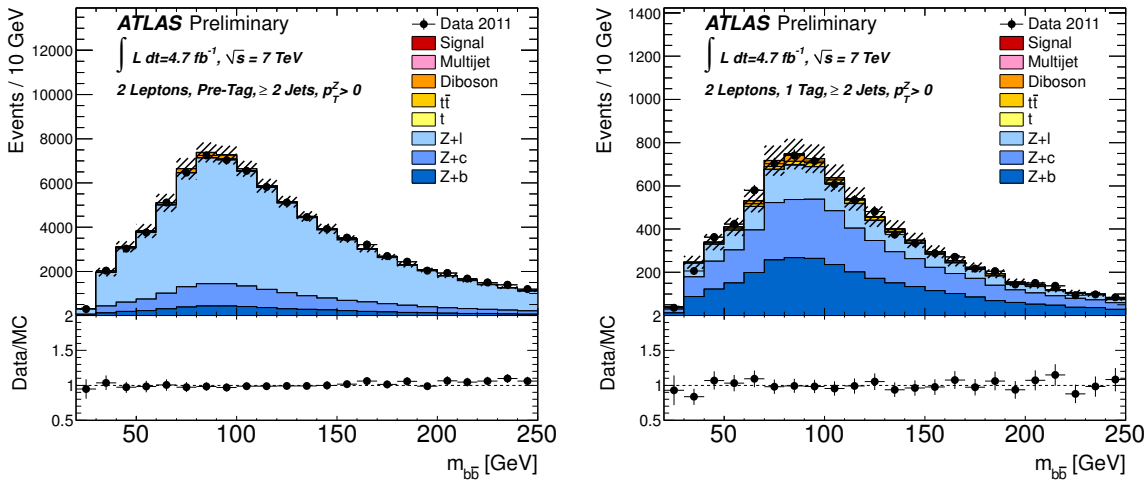

(a) 2-lepton, pre-tag

(b) 2-lepton, 1-tag

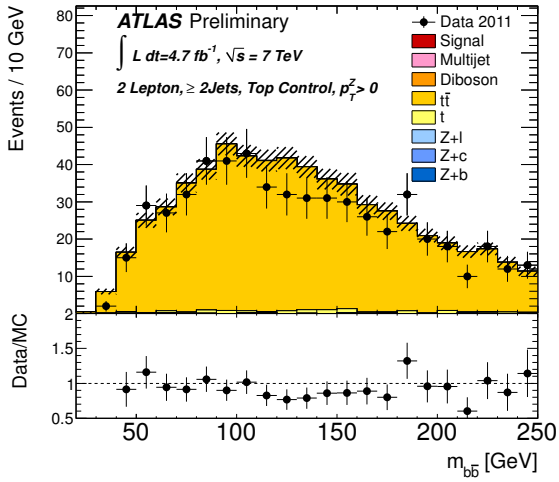

(c) 2-lepton, top control

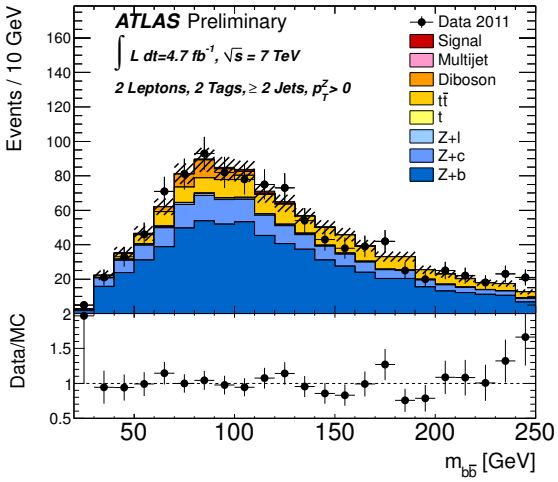

(d) 2-lepton, 2-tag

Figure 15: The control and signal regions for the 0, 1 and 2-lepton selection integrated over the bins of p_{T}^{V} at $\sqrt{s} = 7$ TeV. The error bands indicate the size of the combined statistical and systematic uncertainty before the profile likelihood fit. See text for the precise definition of the control regions.

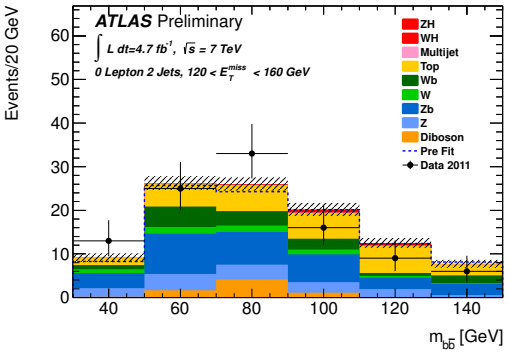

(a) $120 < E_{\mathrm{T}}^{\mathrm{miss}} < 160$ GeV, 2 jets

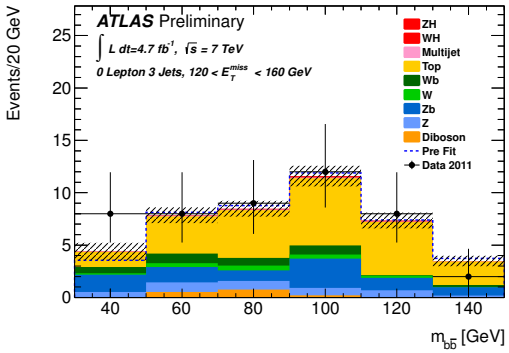

(b) $120 < E_{\mathrm{T}}^{\mathrm{miss}} < 160$ GeV, 3 jets

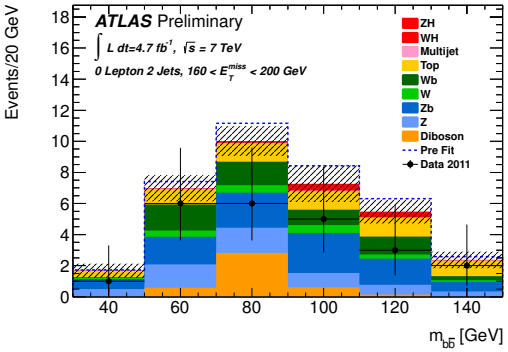

(c) $160 < E_{\mathrm{T}}^{\mathrm{miss}} < 200$ GeV, 2 jets

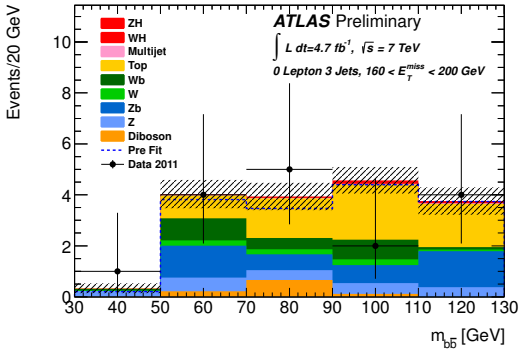

(d) $160 < E_{\mathrm{T}}^{\mathrm{miss}} < 200$ GeV, 3 jets

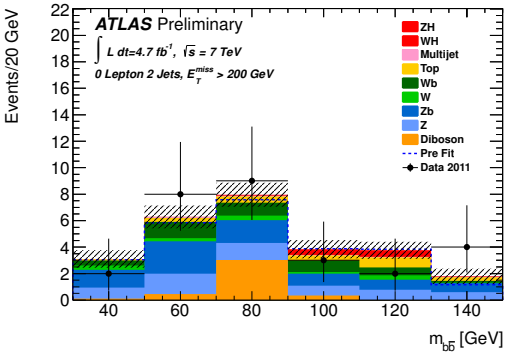

(e) $E_{\mathrm{T}}^{\mathrm{miss}} > 200$ GeV, 2 jets

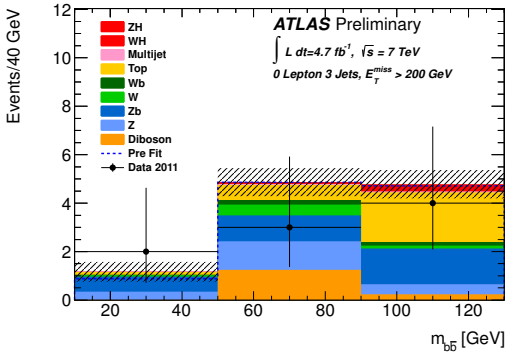

(f) $E_{\mathrm{T}}^{\mathrm{miss}} > 200$ GeV, 3 jets

Figure 16: The $m_{b\bar{b}}$ distribution in data for the six categories of the zero lepton analysis at $\sqrt{s} = 7$ TeV. The background expectation is shown after the profile likelihood fit (solid) and compared to the predictions from the pre-fit Monte Carlo simulation (dashed). The size of the combined statistical and systematic uncertainty is indicated by the hashed band.

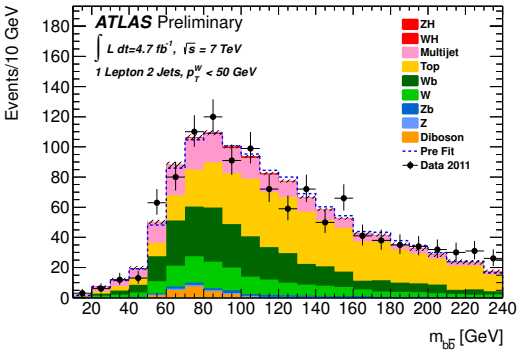

(a) $p_T^W < 50$ GeV

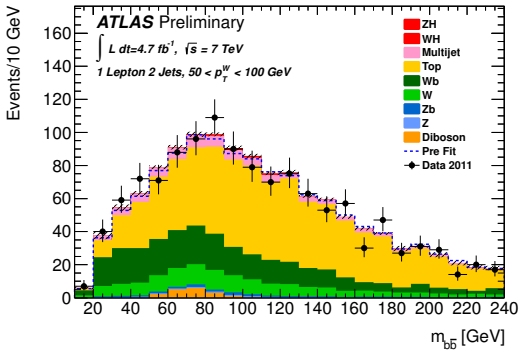

(b) $50 < p_T^W < 100$ GeV

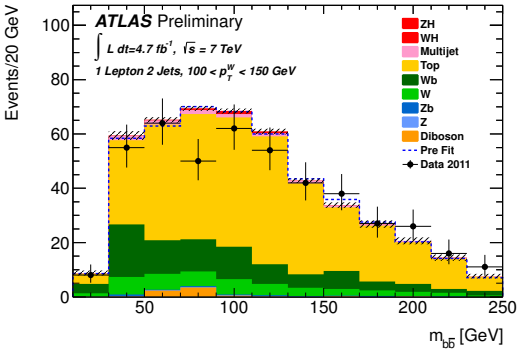

(c) $100 < p_T^W < 150$ GeV

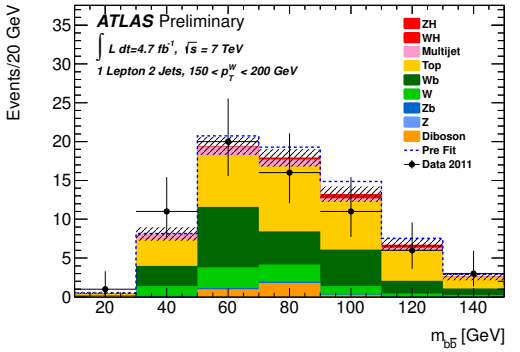

(d) $150 < p_T^W < 200$ GeV

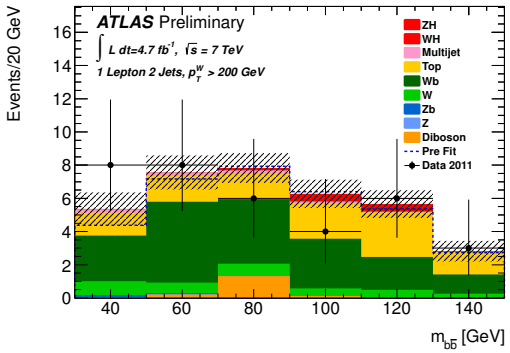

(e) $p_T^W > 200$ GeV

Figure 17: The $m_{b\bar{b}}$ distribution in data for the five categories of the one lepton analysis at $\sqrt{s} = 7$ TeV. The background expectation is shown after the profile likelihood fit (solid) and compared to the predictions from the pre-fit Monte Carlo simulation (dashed). The size of the combined statistical and systematic uncertainty is indicated by the hashed band.

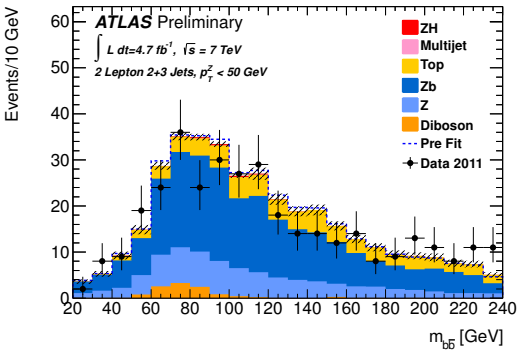

(a) $p_T^Z < 50$ GeV

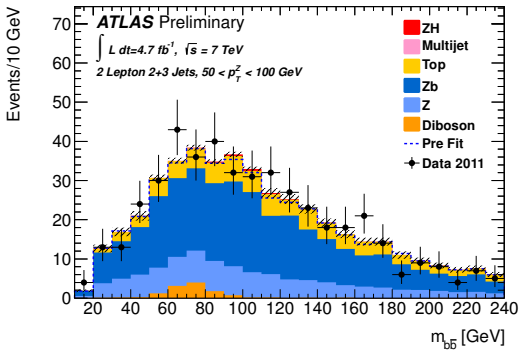

(b) $50 < p_T^Z < 100$ GeV

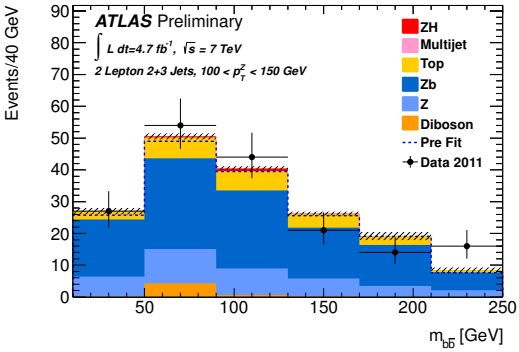

(c) $100 < p_T^Z < 150$ GeV

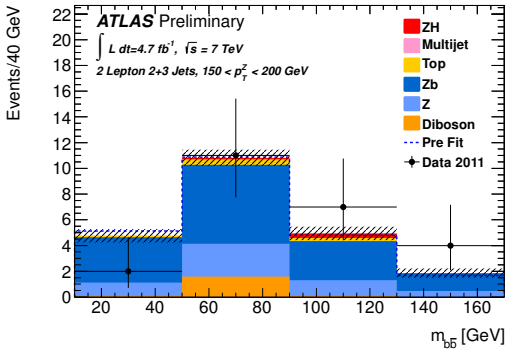

(d) $150 < p_T^Z < 200$ GeV

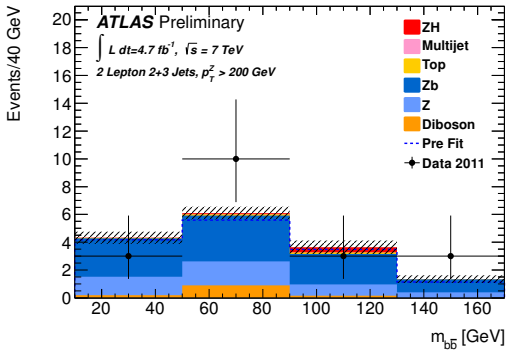

(e) $p_T^Z > 200$ GeV

Figure 18: The $m_{b\bar{b}}$ distribution in data for the five categories of the two lepton analysis at $\sqrt{s} = 7$ TeV. The background expectation is shown after the profile likelihood fit (solid) and compared to the predictions from the pre-fit Monte Carlo simulation (dashed). The size of the combined statistical and systematic uncertainty is indicated by the hashed band.

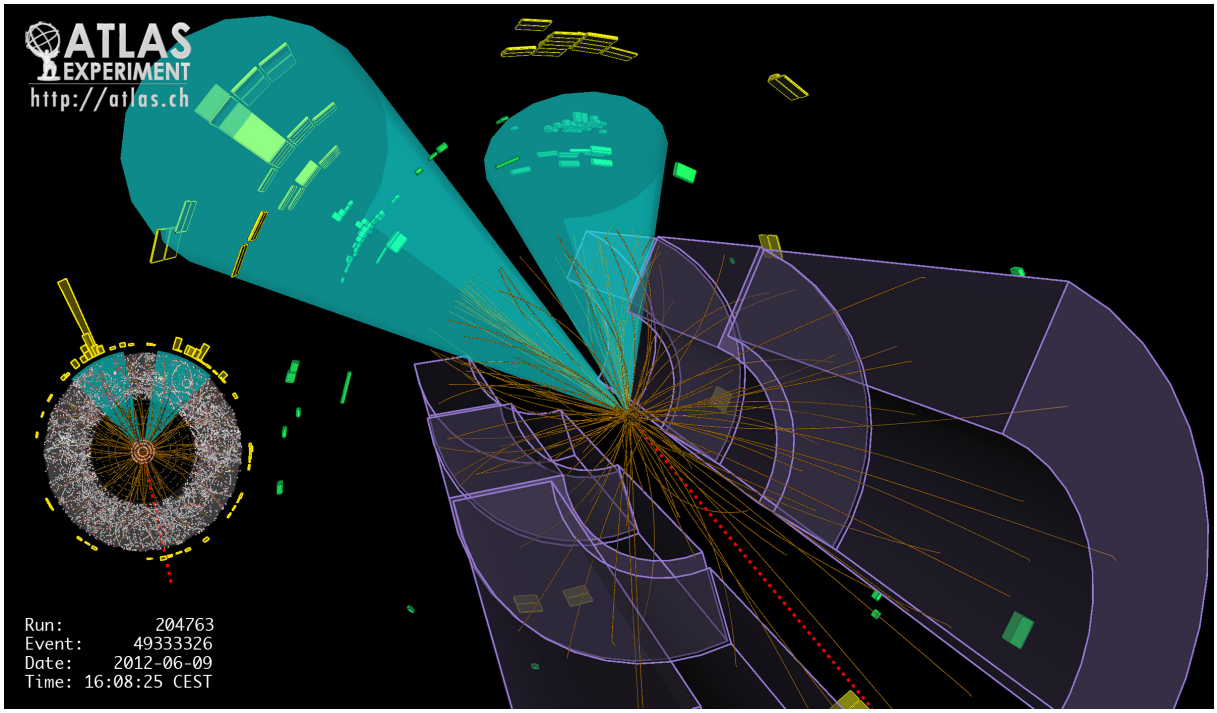

Figure 19: Display of a Higgs boson candidate event with zero selected leptons. The event contains two identified b-jets with transverse momenta of 193 GeV and 78 GeV, respectively, with an invariant mass of 123 GeV. The missing energy in the transverse plane is 271 GeV.

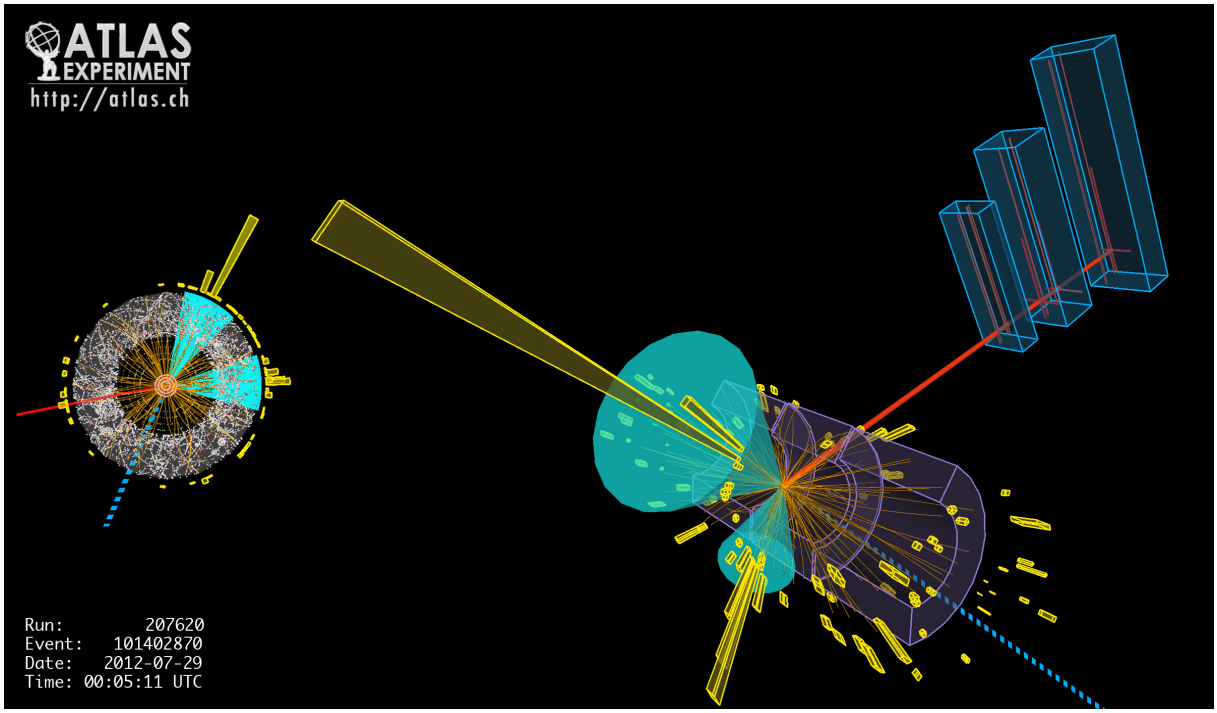

Figure 20: Display of a Higgs boson candidate event with one selected lepton. The two identified b-jets have transverse momenta of 149 GeV and 86 GeV, respectively, with an invariant mass of 109 GeV. The identified muon has a transverse momentum of 96 GeV, the missing energy in the transverse plane is 139 GeV, resulting in a transverse momentum of the W boson candidate of 209 GeV.

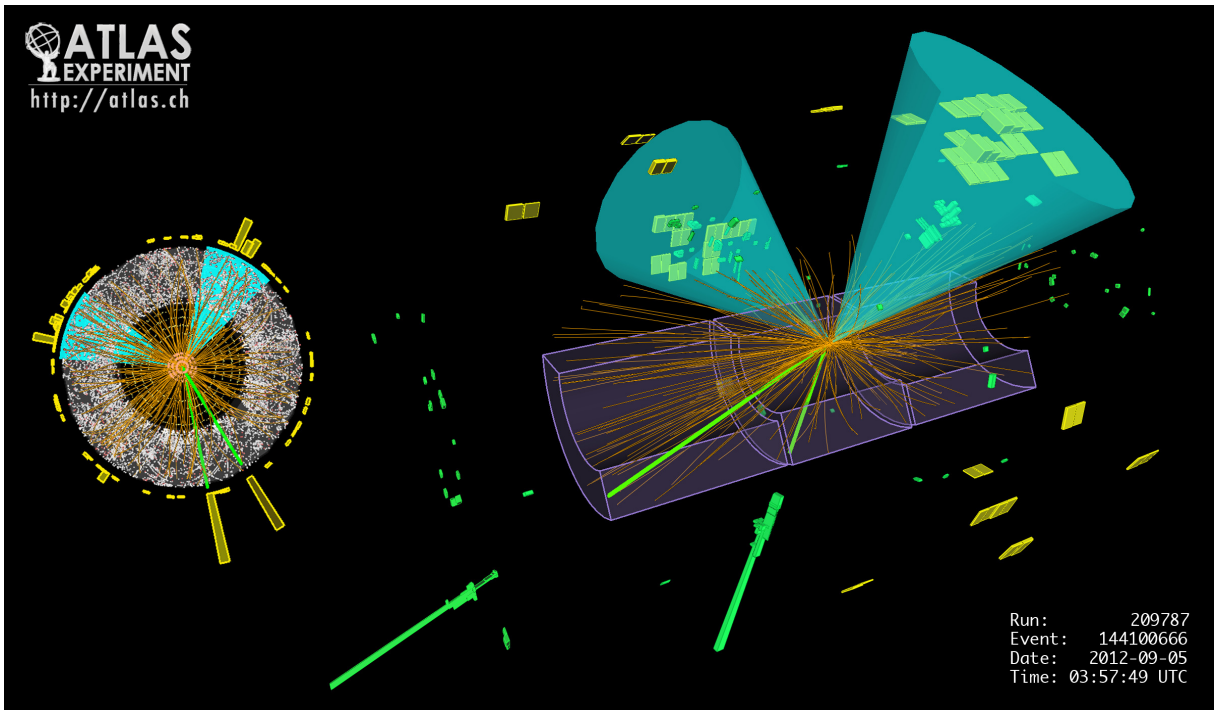

Figure 21: Display of a Higgs boson candidate event with two selected leptons. The two identified b-jets have transverse momenta of 70 GeV and 65 GeV, respectively, with an invariant mass of 122 GeV. The identified electrons have transverse momenta of 63 GeV and 54 GeV, respectively, resulting in a transverse momentum of the Z boson candidate of 115 GeV.